Solar particle penetration into magnetosphere.

K. Kudela, IEP SAS Košice, Slovakia, kkudela@kosice.upjs.sk

Sofia, February 19-20, 2007

1. Ground level events.

Charged particles (mainly protons, heavier nuclei) during some of the solar flares and/or in interplanetary space are accelerated to high energy (rigidity), penetrating into the magnetosphere and producing secondary particles observable at the ground (neutron monitors, muon telescopes occasionally).

First GLE was observed by S.E. Forbush in 1942 (30 years after discovery of cosmic rays by V.Hess) GLE No 1.Spectra different from that of GCR. (copied from *Cosmic Rays, the Sun and Geomagnetism, The works of Scott E. Forbush, J.A. Van Allen, Editor, AGU 1993*).

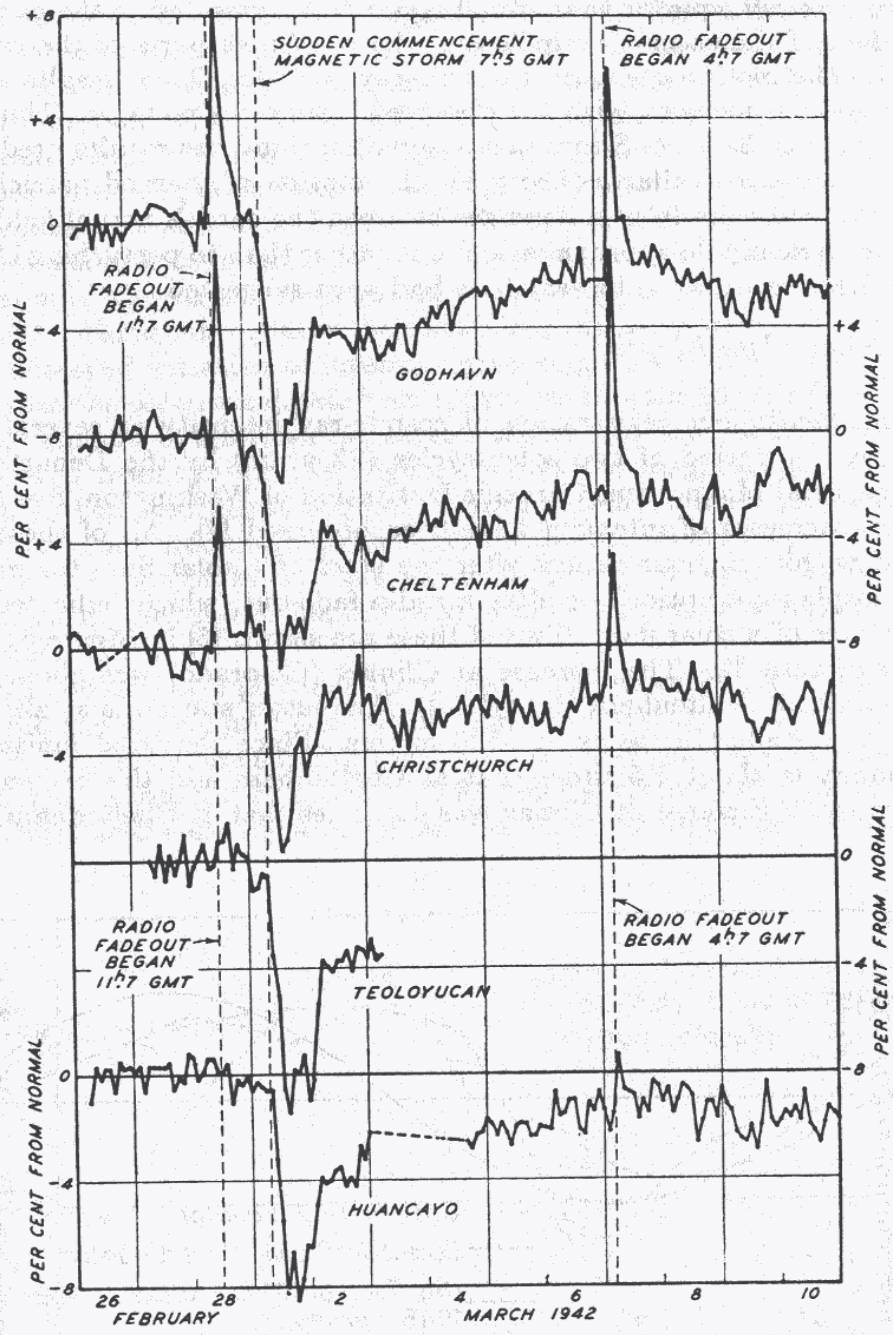

Increases of cosmic-ray intensity, February 28 and March 7, 1942.

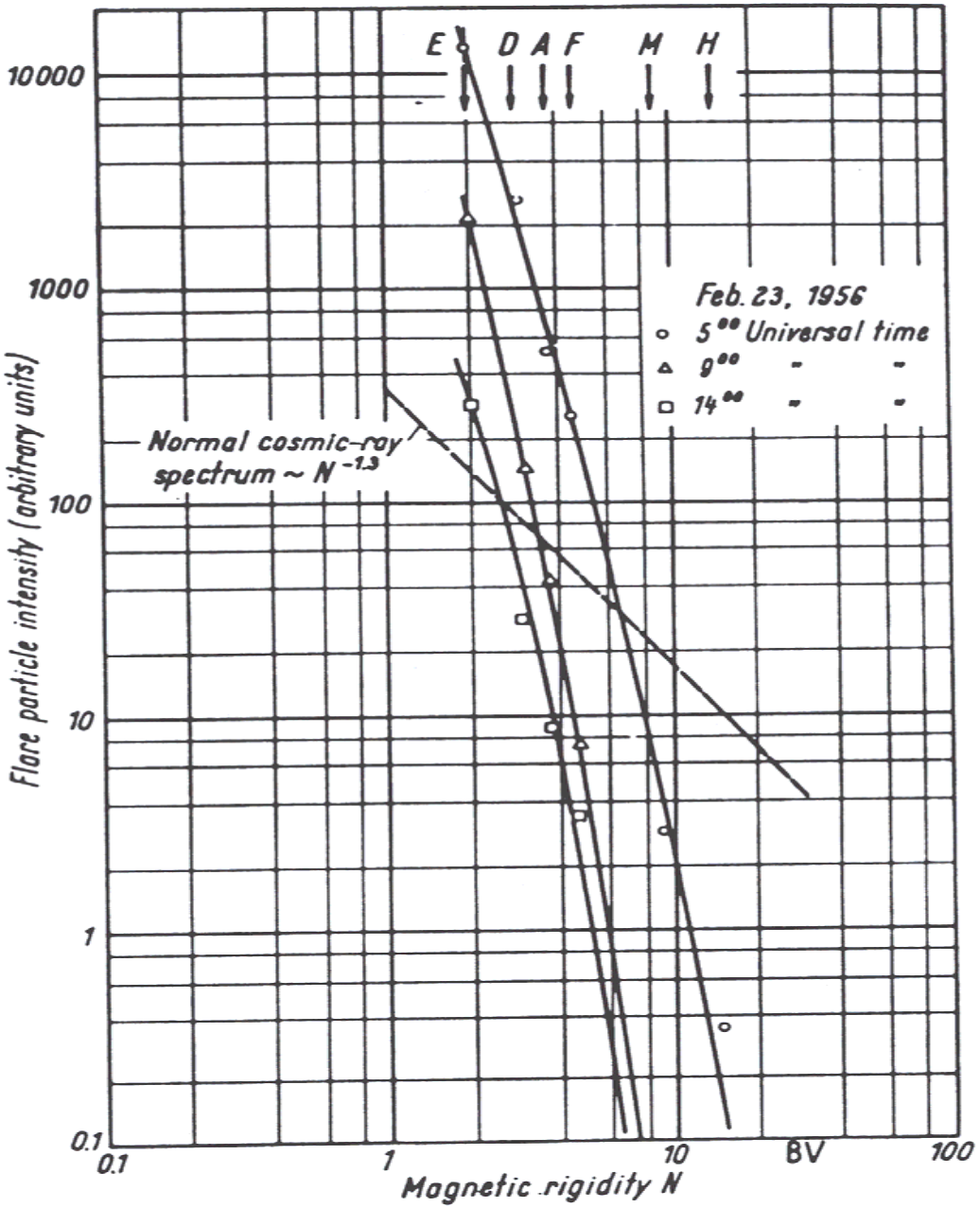

Fig. 82. The differential magnetic rigidity spectrum for the solar protons after particle storage or trapping in the solar system had taken over. Here the particle magnetic rigidity $N = p\,c/Z\,e$, where p is momentum, c is velocity of light, $Z\,e$ is the particle charge, and N is measured in volts. The scale is given in BV = billion volts = 10^9 V (after Simpson et al.).

Spectra of solar cosmic rays observed as Ground Level Events are much softer than those of Galactic CR. However, at stations with low cut-off rigidities they can yield to substantial increases as it was the case of very large GLE in February 1956.

GLE events – catalogue List of GLE events in chronological order (5 – 58) at http://aadc-maps.aad.gov.au/aadc/gle/events.cfm (data and plots collected from many stations).

List of GLEs 55–67 (No 67 Nov. 2, 2003) is e.g. in paper (*Storini et al., Adv. Space Res., 35, 416-420, 2004)*. Two examples of GLE from Lomnický Štít NM (vertical cut-off ~4GV):

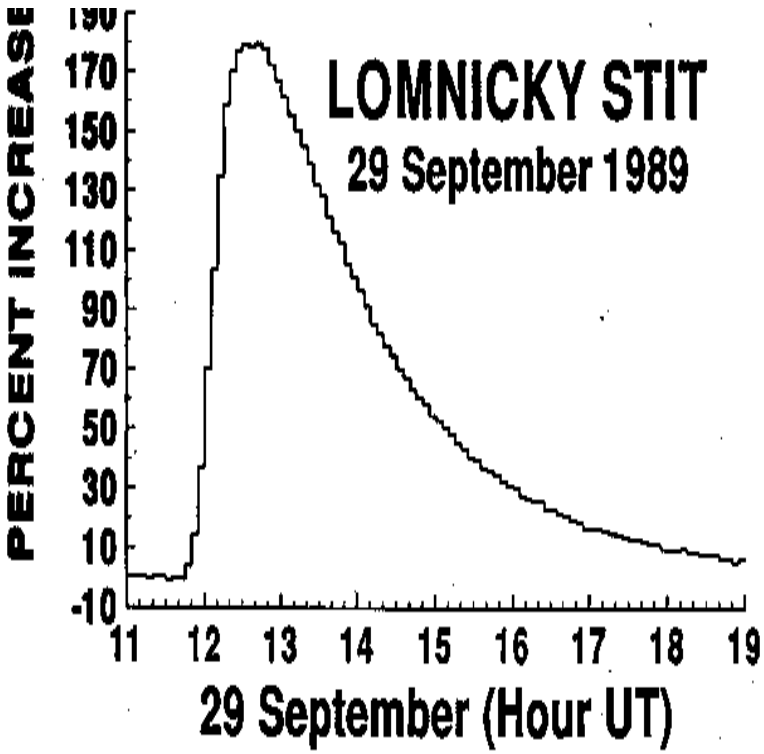

The largest increase from GLE observed at Lomnický Štít (since 1958)

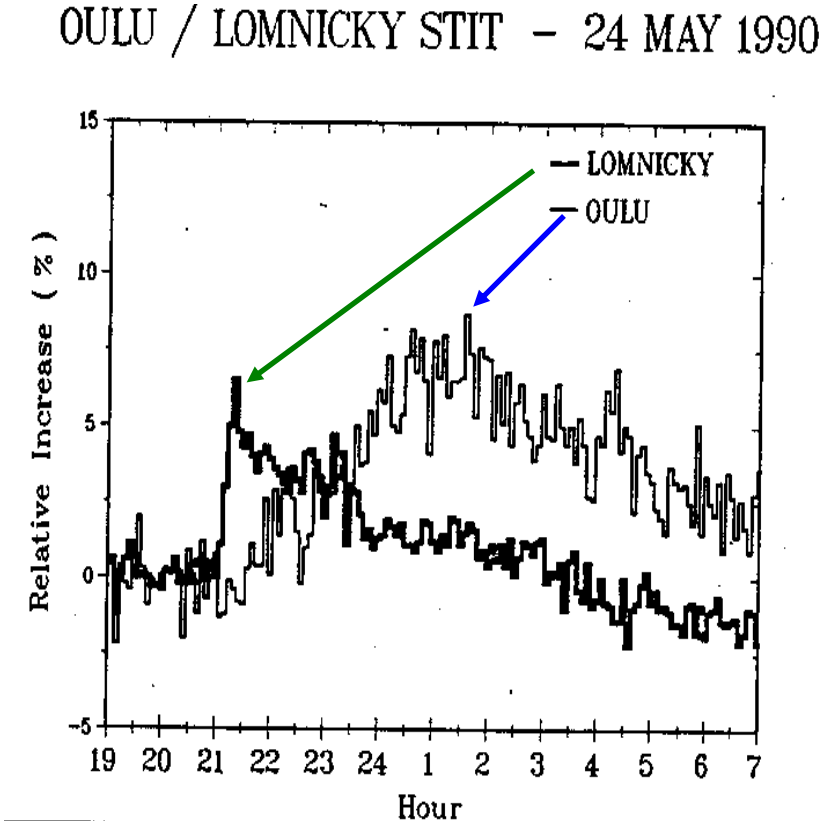

Strongly anisotropic event

1. 2. Neutron monitor.

(portions adapted from Simpson, J.A., "Cosmic-Radiation Neutron Intensity Monitor", in Annals of the IGY, 1955)

The purpose of the neutron monitor is to detect, deep within the atmosphere, variations of intensity in the interplanetary cosmic ray spectrum. Interactions of the primary cosmic rays with the atmosphere produce, among other things, a lower energy secondary nucleonic component consisting of nucleons (expand image at left), in particular neutrons that are not slowed by ionization loss, These secondaries fall in the energy range of a few hundred MeV up to about one GeV. Because of the falling energy spectrum of the primary cosmic rays, the neutron monitors are most sensitive to the low energy (1-20 Gev)portion of the spectrum.

These nucleons in turn produce further nuclear interactions, either in the atmosphere, or in lead target material surrounding the monitor. The interaction rate may be measured most conveniently and reliably by detecting the reaction product neutrons rather than by detecting the charged fragments directly.

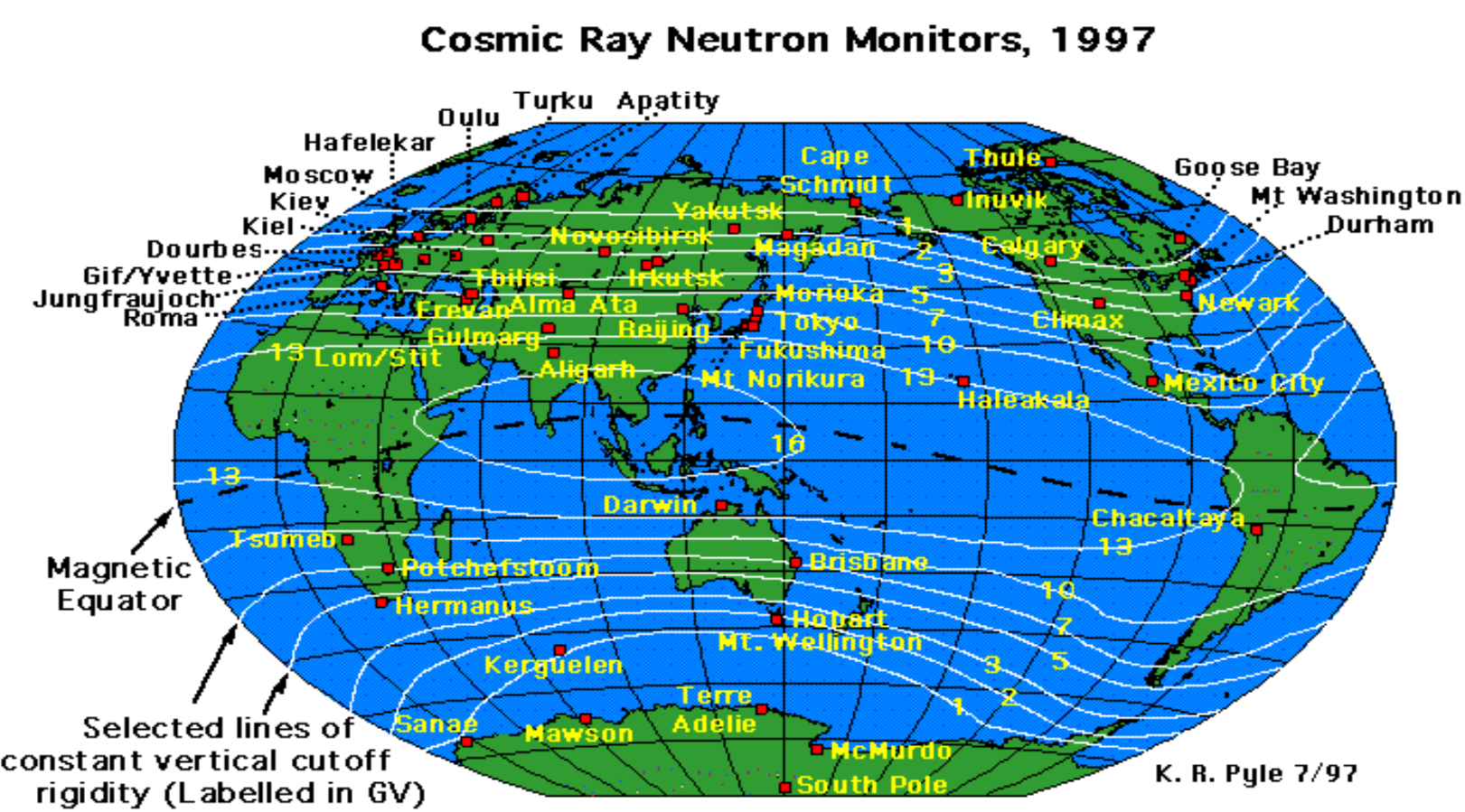

The development of the neutron monitor(NM) by J. A. Simpson (Simpson,1957) provided an improved method of detecting low-energy neutron secondaries that are not slowed by ionization loss. These secondaries fall in the energy range of a few hundred MeV up to about one GeV. *NMs are most sensitive to the low energy (1-20 GeV) portion of the spectrum*. NMs with their reliability and basic simplicity offered a means of studying the longer-term temporal variations while their sensitivity and high counting rates made possible the observation of short term intensity changes as well.

High altitude NMs are important (statistical acurracy) if compared with low altitudes.

TABLE 1

Neutron monitors with the highest counting rate

Station	Lat. (deg)	Alt. (m)	Press. (mb)	Cutoff (GV)	Counting rate s^{-1}	Statist. rank
Tibet	30.1	4300	606	14.1	2970	1.00
Alma Ata B	43.3	3340	680	6.61	1285	0.64
Erevun	40.2	2000	815	7.58	1100	0.61
Haleakala	20.7	3030	700	12.9	970	0.57
Lomnicky Stit	49.2	2634	748	3.98	420	0.38
Jungfraujoch 2	46.5	3475	646	4.61	390	0.33
Tsumeb	−19.2	1240	880	9.21	310	0.33
Calgary	51.1	1128	883	1.08	270	0.30
South Pole	−90.0	2820	680	0.09	260	0.29
Irkutsk 3	52.3	3000	715	3.64	240	0.28
McMurdo	−77.9	48	1007	0	230	0.28
Irkutsk 2	52.3	2000	800	3.64	210	0.26
Moscow	55.5	200	1000	2.43	200	0.26
Kerguelen	−49.4	0	1000	1.14	190	0.25
Inuvik	68.3	21	1010	0.17	160	0.24
Novosibirsk	54.8	163	1000	2.87	160	0.23

Moraal, H. et al., Space Sci. Rev, 2000

NM (8)

One of high mountain NMs is Lomnický štít, data in real time at http://neutronmonitor.ta3.sk

Detail of detectors of neutron monitor. Altogether 8 proportional counters SNM-15 are at Lomnický Štít mountain.

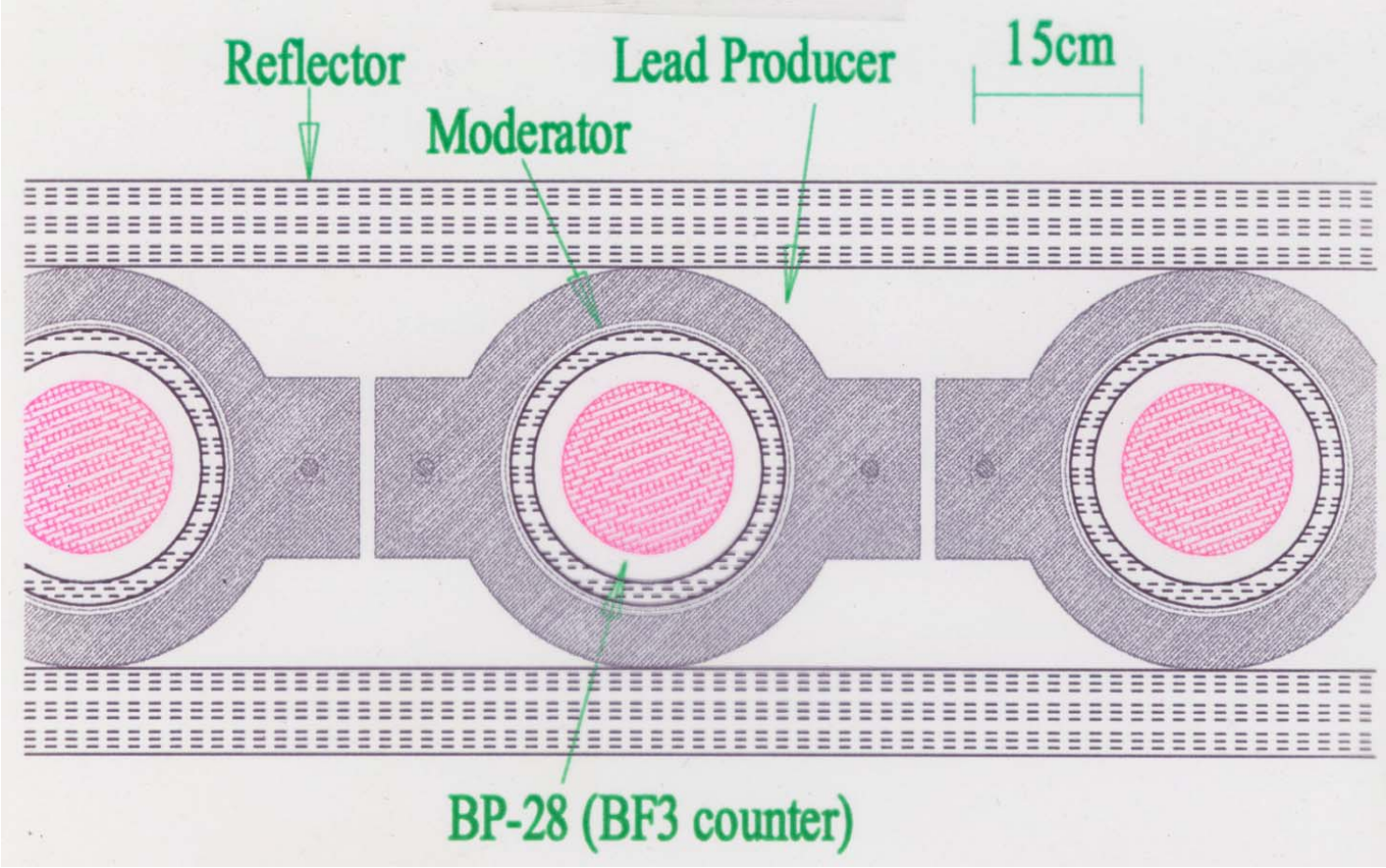

For detection in proportional counters the reactions $^{10}B(n,\alpha)^{7}Li$ **or** $^{3}He(n,p)^{3}H$ are used (high cross section for n reactions of slow n). ***Moderator*** **(**low mass number**)** is slowing down the neutrons (polyethylene or paraffin), ***producer*** of lead is producing multiple neutrons (their number ~ $A^{0.7}$,heavy elements), ***reflector*** maintains the neutrons inside the NM and reflects the outer n of low energy (produced locally not due to cosmic rays). Copied from *J.M. Clem,* http://www.physics.purdue.edu/cronus/files/cronus04.ppt

To convert ground-level particle intensity to NM counting rate the detection efficiency of NM system must be known. A yield function is then determined by calculating the average number of NM counts per incident primary - detection efficiency of primaries.

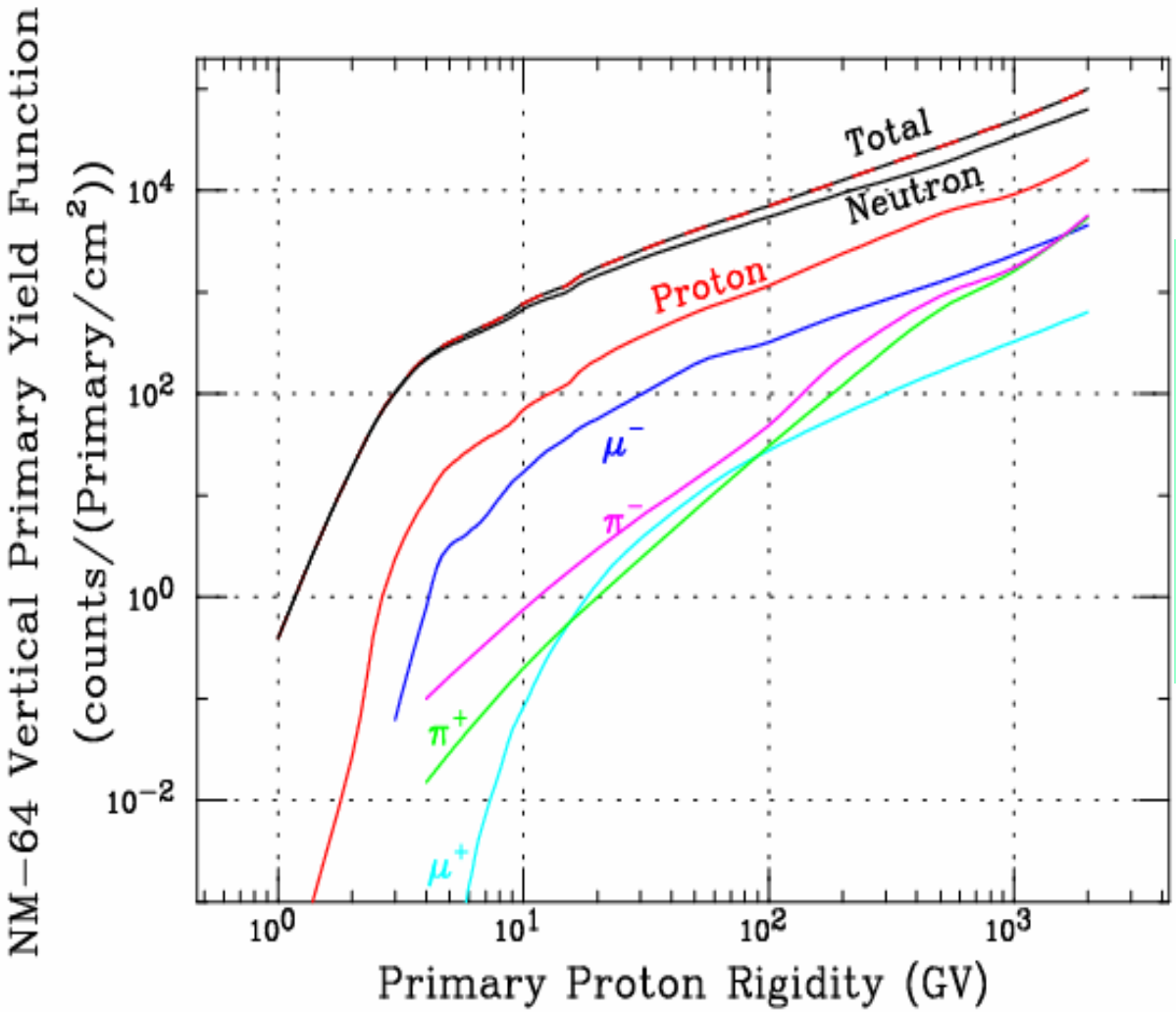

The yield units are average number of NM counts for every incident primary particle per cm^2.

Calculated yield function for vertical incident primary protons at sea level.

From J. Clem, http://www.physics.purdue.edu/cronus/files/cronus04.ppt . More e.g. in paper (*J.M. Clem, L.I. Dorman, Space Sci. Rev., 93, 335-360, 2000*).

Using many cosmic ray NM station records (various positions, different cut-off rigidities and asymptotic directions), IMF measurements, coupling functions of NMs ⇨ rigidity spectra of accelerated particles and apparent source direction can be derived. Example: from (*Cramp J.L.,M.L. Duldig and J.E. Humble, Proc. ICRC Calgary, 1993, vol. 3, p. 47-50*) used 42 neutron monitors for GLE of 29 September 1989.

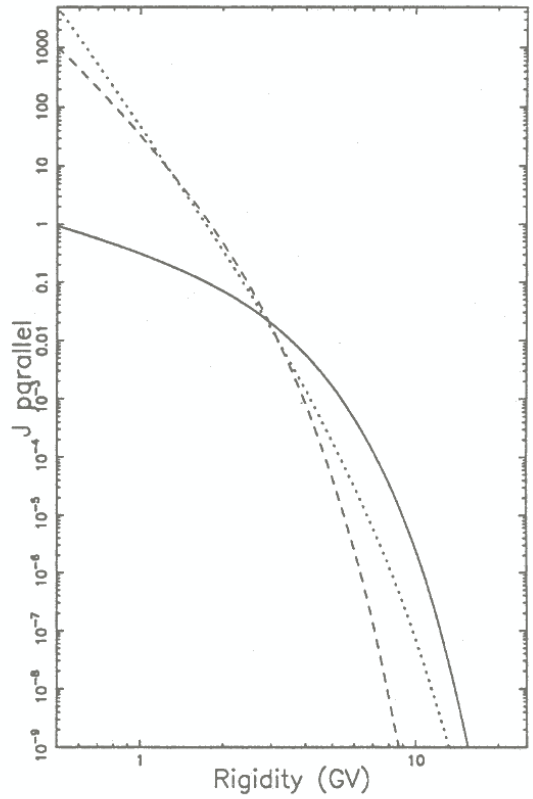

FIG 1. Derived particle specta for 12:15-20UT (solid line), 13:25-30UT (dashed line) and 16:00-05UT (dotted line).

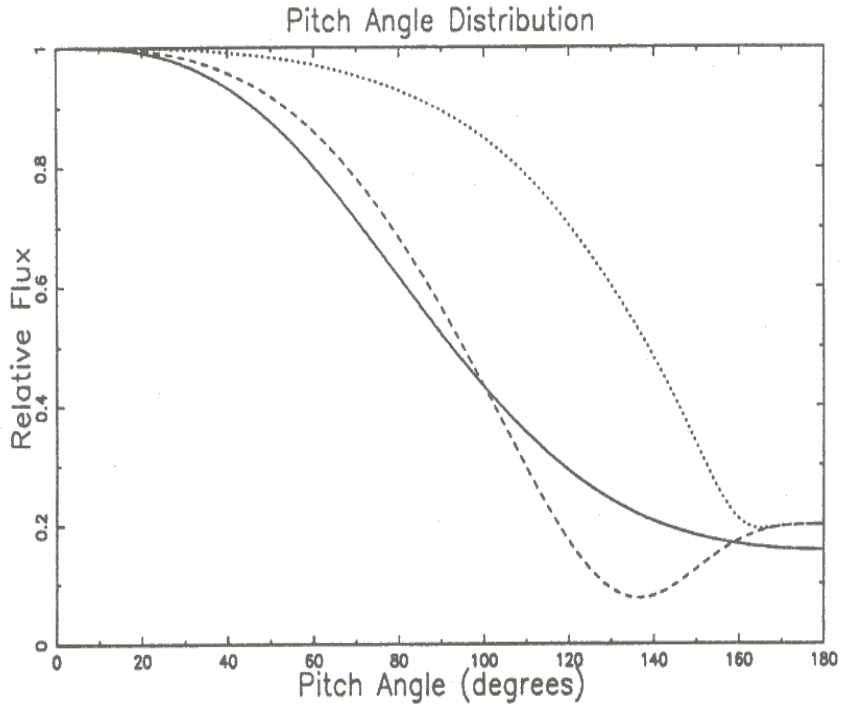

FIG 2. Derived particle pitch angle distributions for 12:15-20UT (solid line), 13:25-30UT (dashed line) and 16:00-05UT (dotted line).

Recently, the GLE on January 20, 2005 was one of the largest since that of February 1956 (e.g. *Bieber, J., et al. Proc. 29th ICRC (Pune), 1, 237-240, 2005*). Neutron monitors have better time resolution now (1 min or even better) in comparison with measurements in 1956.
Observed during a Forbush decrease. The computations of access by (*Flückiger, E.O. et al., Proc. 29th ICRC (Pune), 1, 225-228, 2005*) estimated the energy spectra form and apparent source for different time intervals.

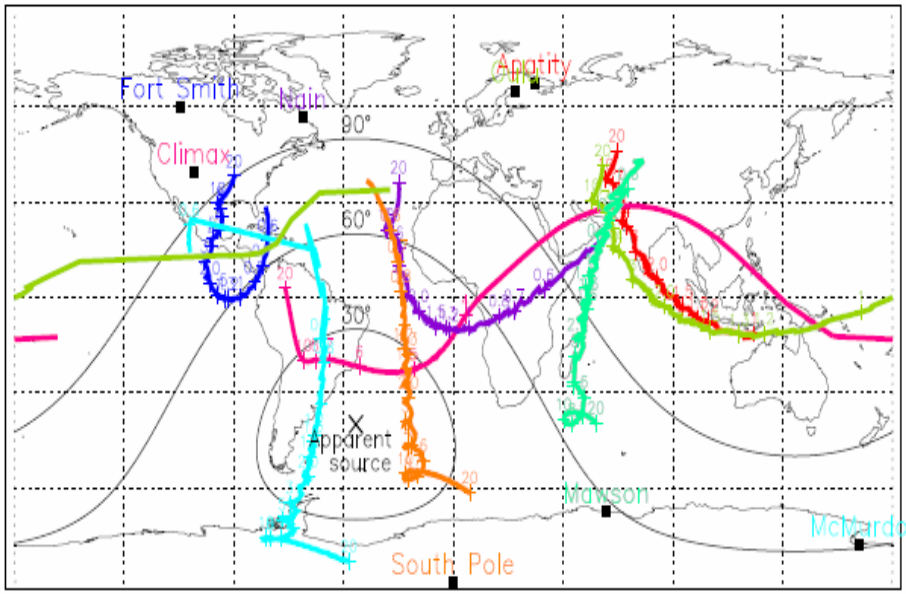

Table 2. Parameters for the January 20, 2005, GLE (preliminary results)

Time	Spectral index	Apparent source	
		Latitude	Longitude
0653–0655	~4.5	-40	310
0655–0657	~7.0	-50	320
0657–0659	~7.0	-40	320
0659–0701	~6.5	-50	310

Asymptotic directions for 0655-0657 UT in GLE January 20, 2005 (*Flückiger E.O. et al., 2005*).

The acceleration was efficient to high energies. The event was anisotropic.

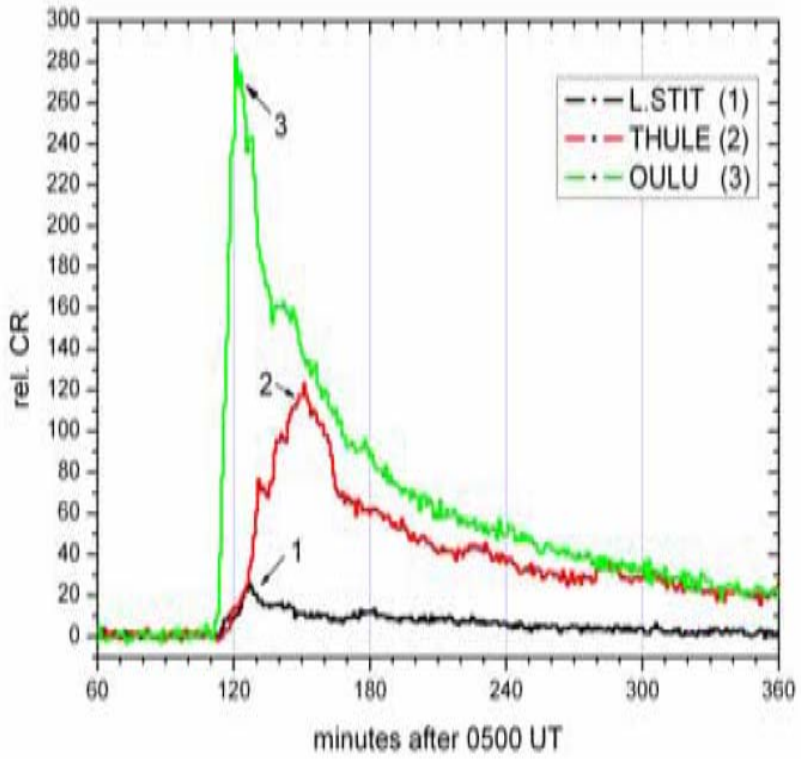

Figure 4. The neutron monitor increases during the event on 20 January 2005. Geomagnetic vertical cutoffs of Lomnický Štít (LS), Oulu and Thule are ~4 GV, 0.8 GV and ~0 GV respectively.

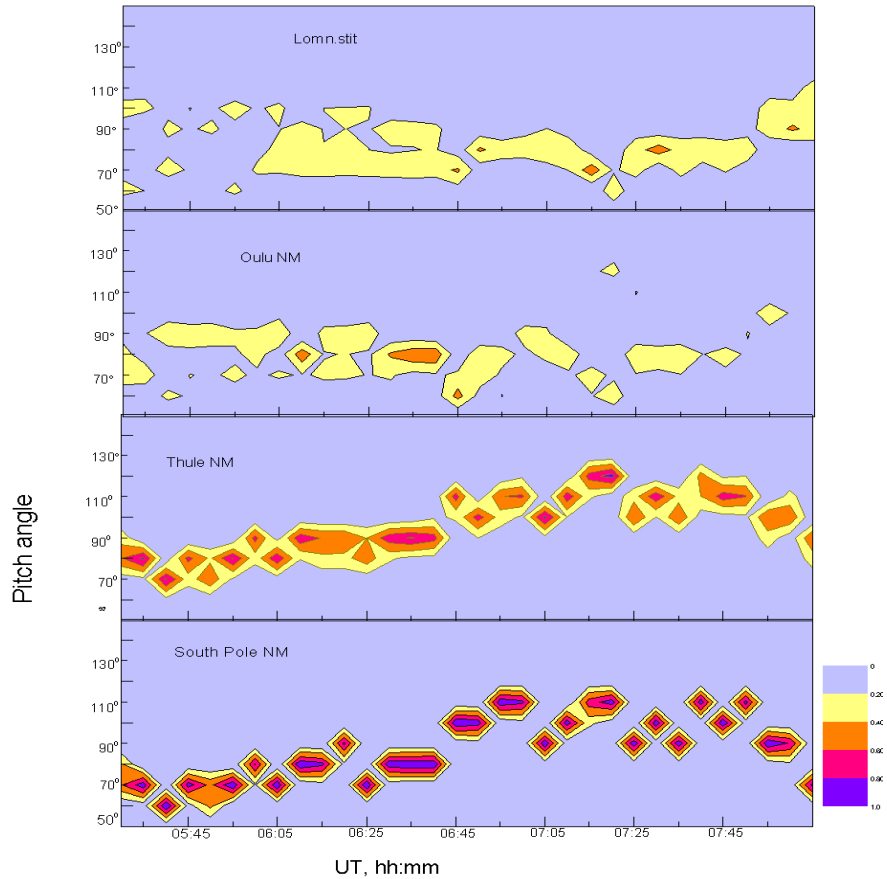

Figure 5. Contributions to the access of cosmic rays with rigidity spectra R^{-5} at 4 NMs on 20 January 2005. For each 5 min interval the computation is based on trajectory tracing (IGRF) and „measuring" the angle between IMF **B** (obtained from ACE web page) and the asymptotic directions. Color code (normalized to unity in 5 min intervals) is the relative contribution to the CR access. South Pole has a very narrow pitch angle acceptance cone.

Kuznetsov S.N. et al., Proc. 29th ICRC (Pune), 1, 49-52, 2005

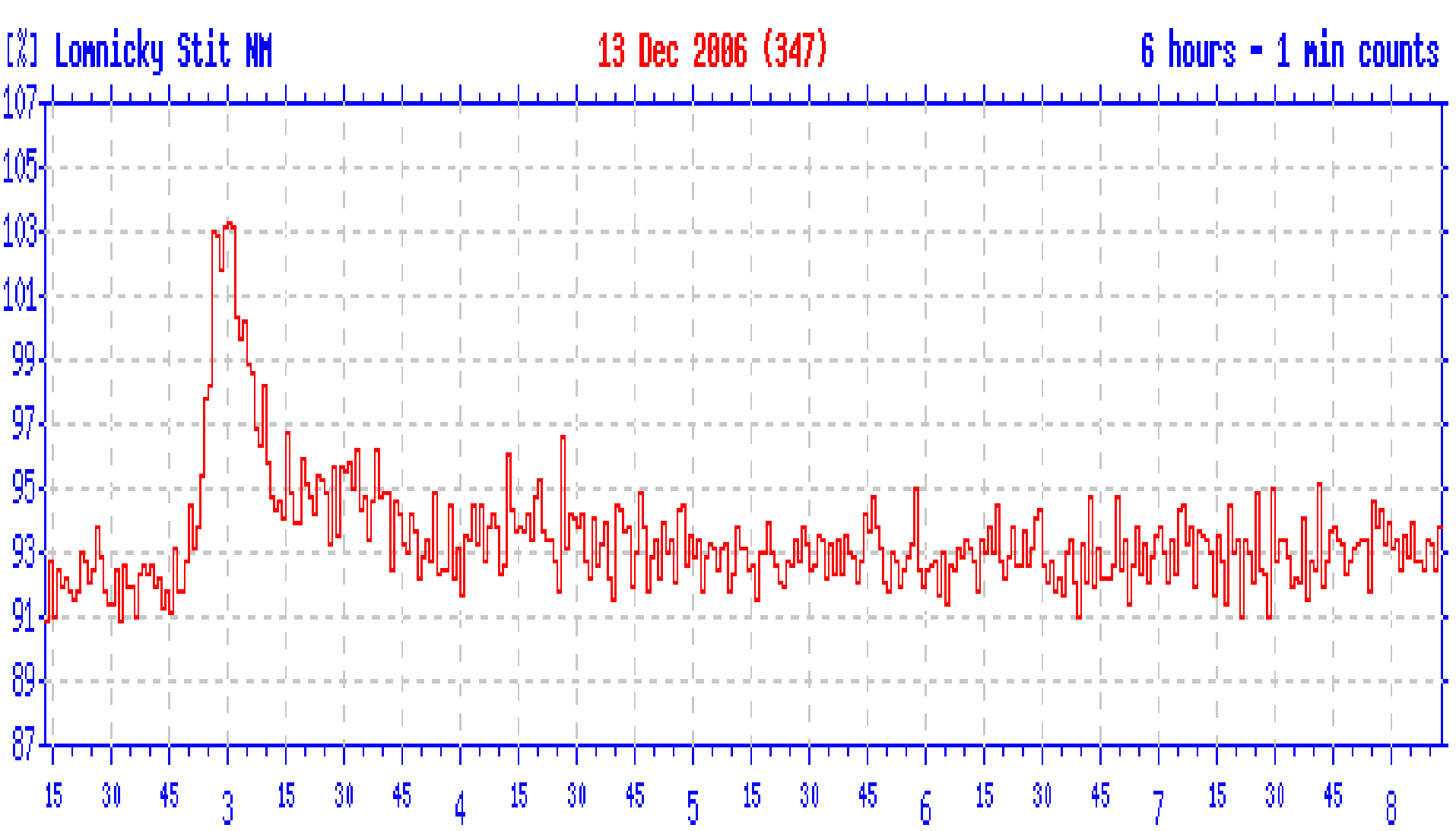

Recent ground level event (GLE 70) observed at

Lomnický Štít, December 13, 2006, 1min data. Time in UT.

1.3. Solar neutrons observed at earth.

Solar neutrons are produced by nuclear interactions of accelerated protons with nuclei of solar atmosphere. Neutrons are decaying

$n \rightarrow p + e^- + \bar{\nu}$ (lifetime of n is ~ 14.8 min)

First response of solar neutrons on the ground was from flare on June 3, 1982 (***Jungfraujoch and Lomnický Štít NMs***). Not affected by IMF.

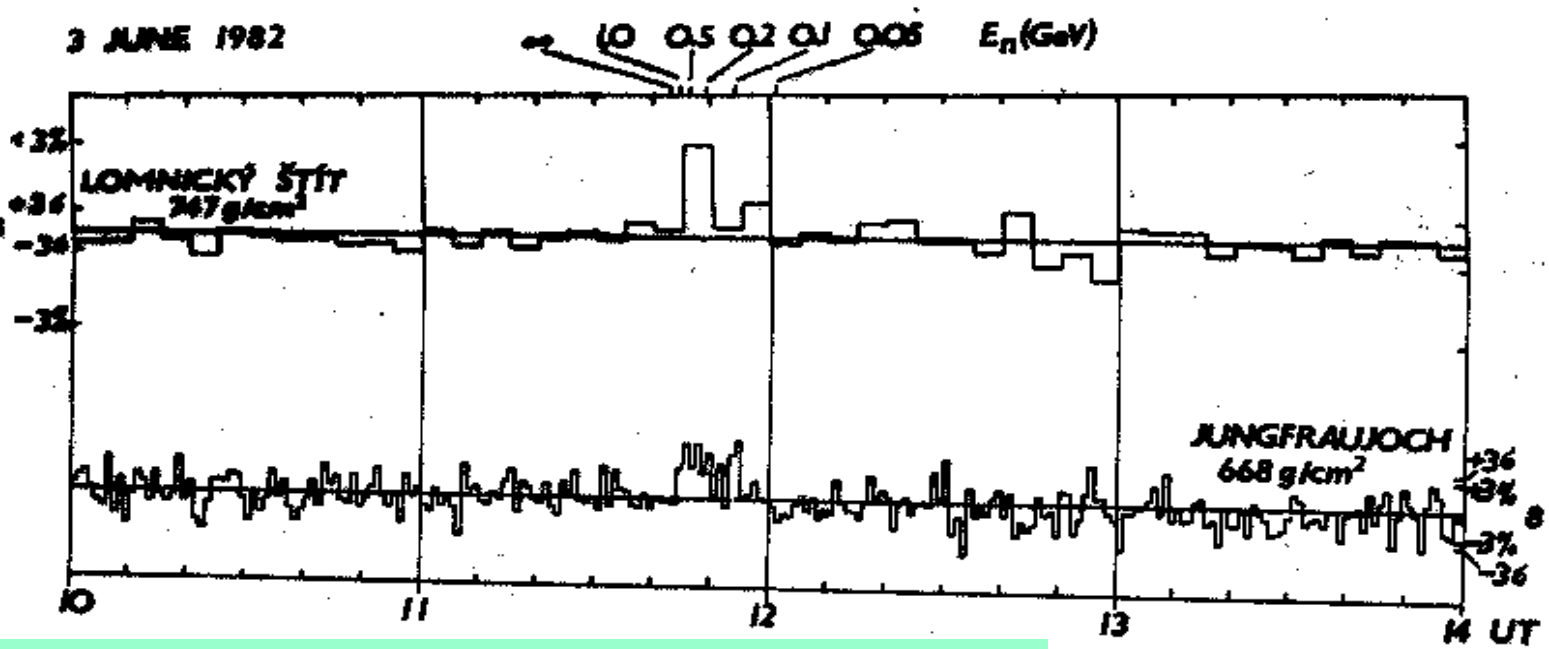

Efimov,Y.E, Kocharov,G.E, Kudela, K., Proc. ICRC, Bangalore, 10, 276-279, 1983

first ground-based observation of solar neutrons

Most important sources of solar neutrons (cross sections of reactions of p and α particles with constituents of solar surface are e.g. in paper (*Murphy, R.J. , C.D. Dermer and R. Ramaty, Astrophys. J. Suppl. 63, 721, 1987*).

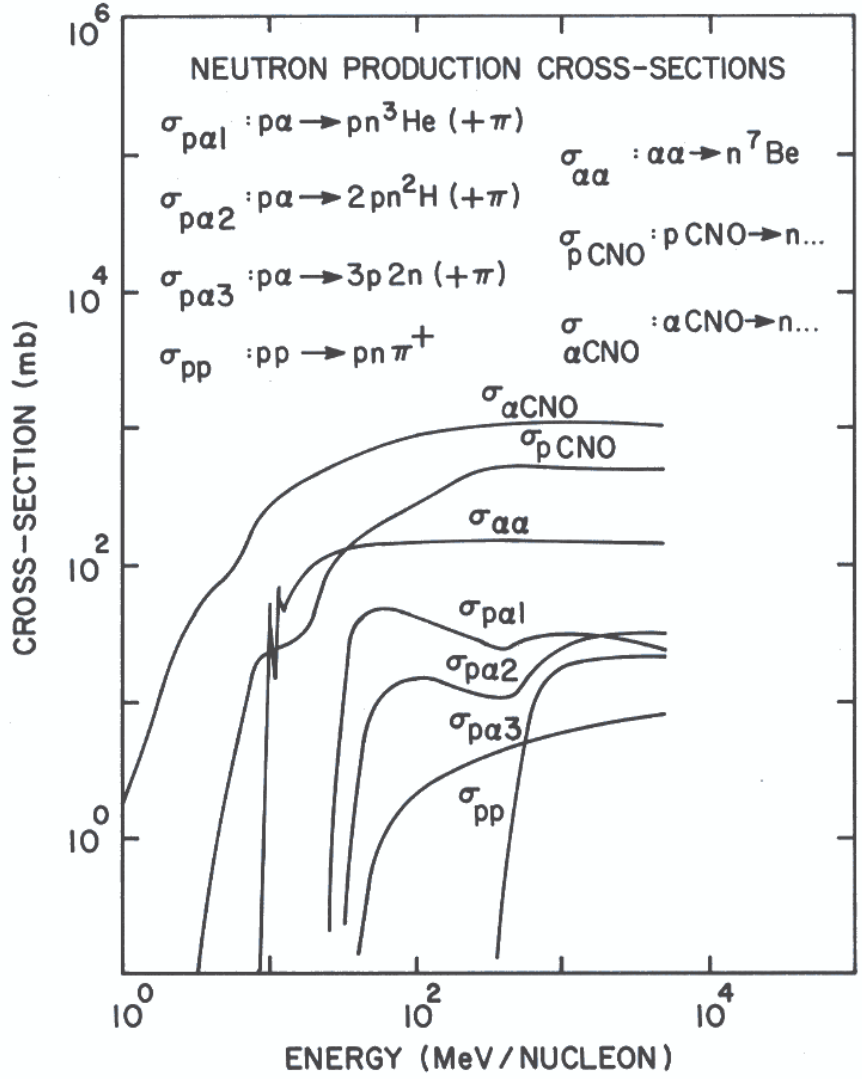

Fig. 2. The cross-section for neutron production on the ambient solar constituents versus proton or α particle energy (MeV nucleon)$^{-1}$. After Murphy, Dermer, and Ramaty (1987).

Neutron production spectra are calculated based on assumptions of p accelerated spectra, cross sections of pp, pα, $\alpha\alpha$ reactions, interactions with heavier nuclei, ambient abundance.

Solar neutrons are studied on the ground (mountains).

Survey of solar neutron events in cycle 23 by (*Watanabe K. et al, Proc. ICRC, Pune, 1, 37-40, 2005)*

Table 2. Summary and results of the analysis of the solar neutron events in solar cycle 23, including information on the solar flares and observatories, energy spectrum and flux of solar neutrons.

Date	Nov 24, 2000	Aug 25, 2001	Oct 28, 2003	Nov 2, 2003	Nov 4, 2003
Flare Start Time [UT]	14:51	16:23	9:51	17:03	19:29
GOES X-ray class	X2.3	X5.3	X17.4	X8.3	X28
Sunspot location	N22 W07	S17 E34	S16 E08	S14 W56	S19 W83
Observatory	Chacaltaya (Bolivia)	Chacaltaya (Bolivia)	Tsumeb (Namibia)	Chacaltaya (Bolivia)	Haleakala (Hawaii, USA)
Height [m]	5250	5250	1240	5250	3030
Detector	12NM64	12NM64	18NM64	12NM64	18NM64
Flux at 100 MeV [$\times 10^{28}$ /MeV/sr]	0.04 ± 0.01	0.02 ± 0.01	0.37 ± 0.14	0.03 ± 0.01	1.5 ± 0.6
Power index	-4.2 ± 0.5	-3.1 ± 0.4	-3.8 ± 0.4	-7.0 ± 1.3	-3.9 ± 0.5
Neutron flux [/sr]	8.0×10^{28}	4.1×10^{28}	1.2×10^{29}	2.8×10^{29}	2.4×10^{30}
at the Sun [erg/sr]	1.0×10^{25}	6.4×10^{24}	3.3×10^{25}	2.6×10^{25}	3.4×10^{26}

Example (students):

what is the probability that solar neutron with kinetic energy 10 MeV, 100 MeV, 1 GeV arrives to earth orbit without decay and what is the time delay between its production and detection near Earth.

2. Observations of solar energetic particles by satellites.

Low altitude orbits, especially those with high inclinations, are useful for checking of cut-off invariant latitudes (or L) in magnetosphere, to which the energetic particles accelerated at solar surface and/or in interplanetary space are penetrating. Rather good temporal resolution. Single experiment – no problems with intercalibration as it is the case with ground experiments.

2.1. Charged energetic particles.

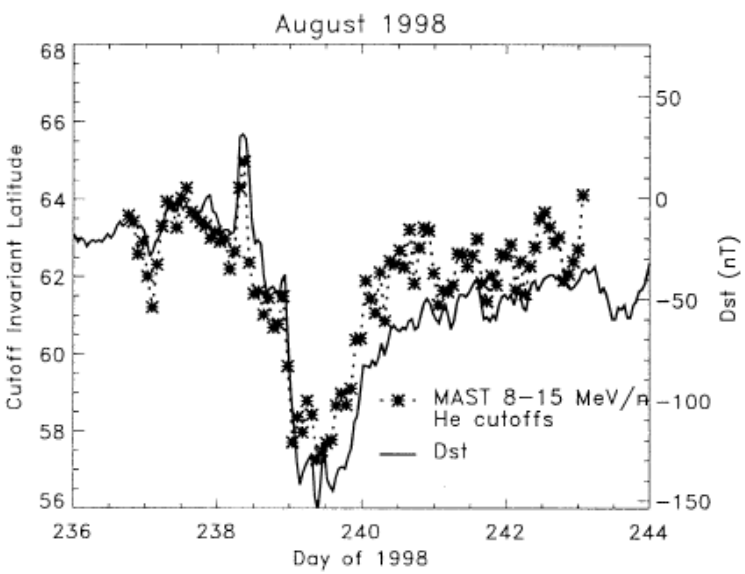

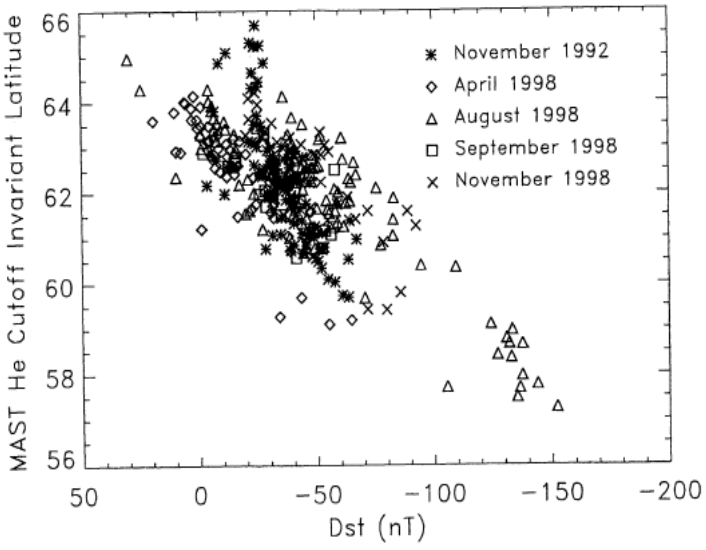

. Orbit-averaged cutoff invariant latitude for ~ 8-15 MeV/nucleon He
olated to the same time as the cutoff measurement, for the five time peri

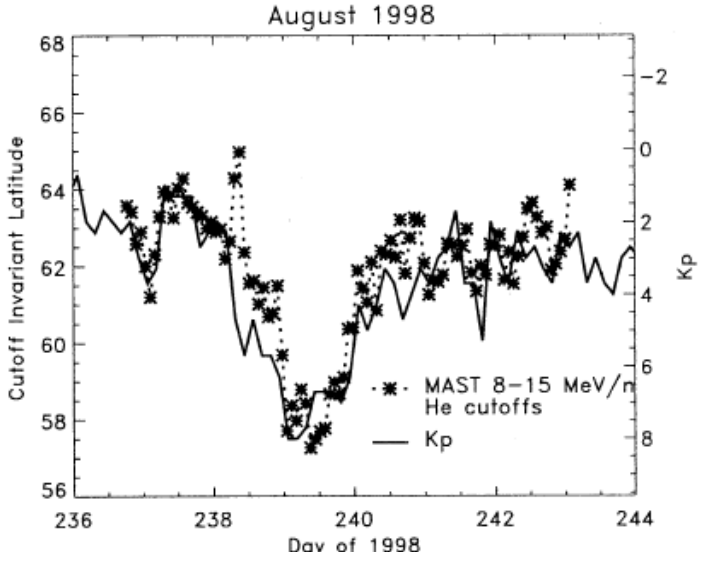

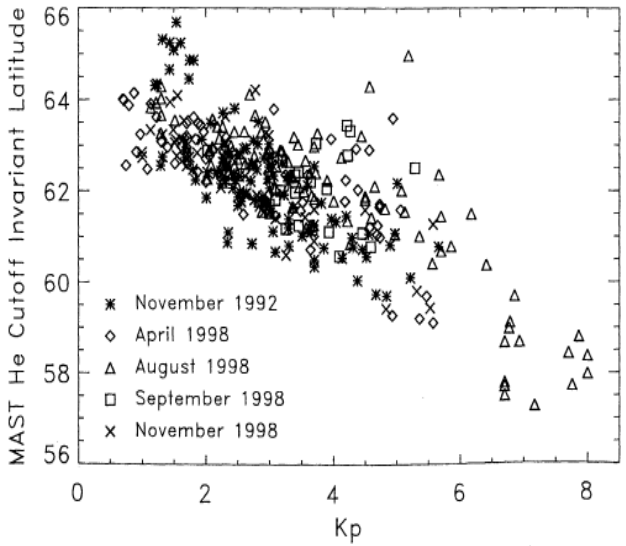

Figure 6. Orbit-averaged cutoff invariant latitude for ~ 8-15 MeV/nucleon He plotted versus *Kp* interpolated to the same time as the cutoff measurement, for the five time periods indicated.

From (*Leske et al., JGR, 106, A12, 30,011-30,022, 2001*): Cut-off invariant latitude for penetration of solar cosmic rays (He ~8-15 MeV) to SAMPEX orbit depends on Kp and on Dst.

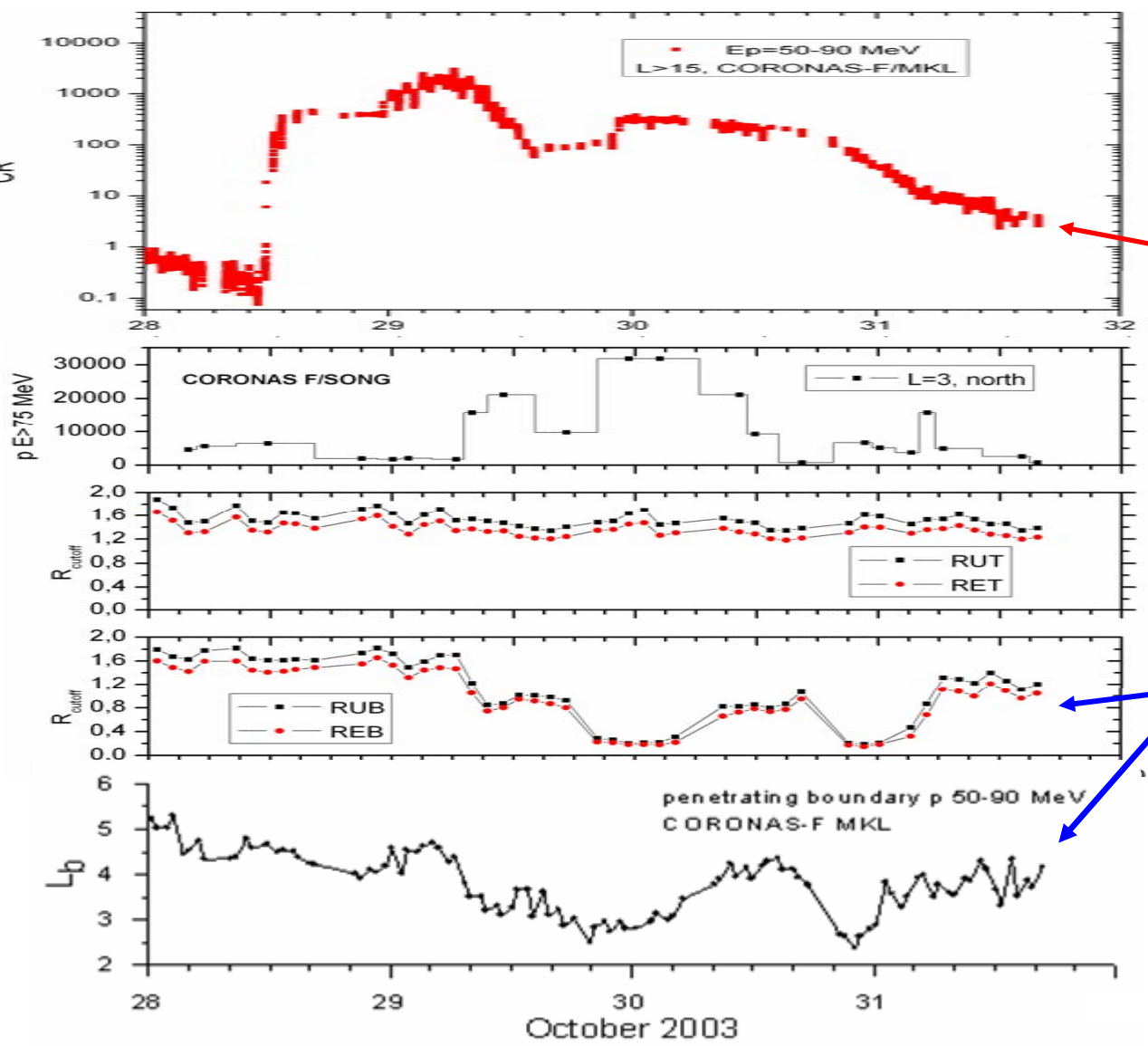

From *(Kuznetsov S.N., et al, ICRC Pune, 2, 409-412, 2005)*.

At high latitude passes of CORONAS-F the energetic protons accelerated during the solar flare are seen.

Particles *penetrate to lower L shells due to improved geomagnetic transmissivity.*

Figure 2. The event on October 28 seen at high latitudes (L>15 selections, upper panels) and at L=3 in the northern hemisphere (3rd and 4th panel). The two lowest panels show the expected vertical cutoffs (Ts 89[16] and Ts89+Dst [13]). The largest increase at L=3 by MKL and SONG (>75 MeV) approximately corresponds to the lowest Dst and to lowest cutoffs expecteded.

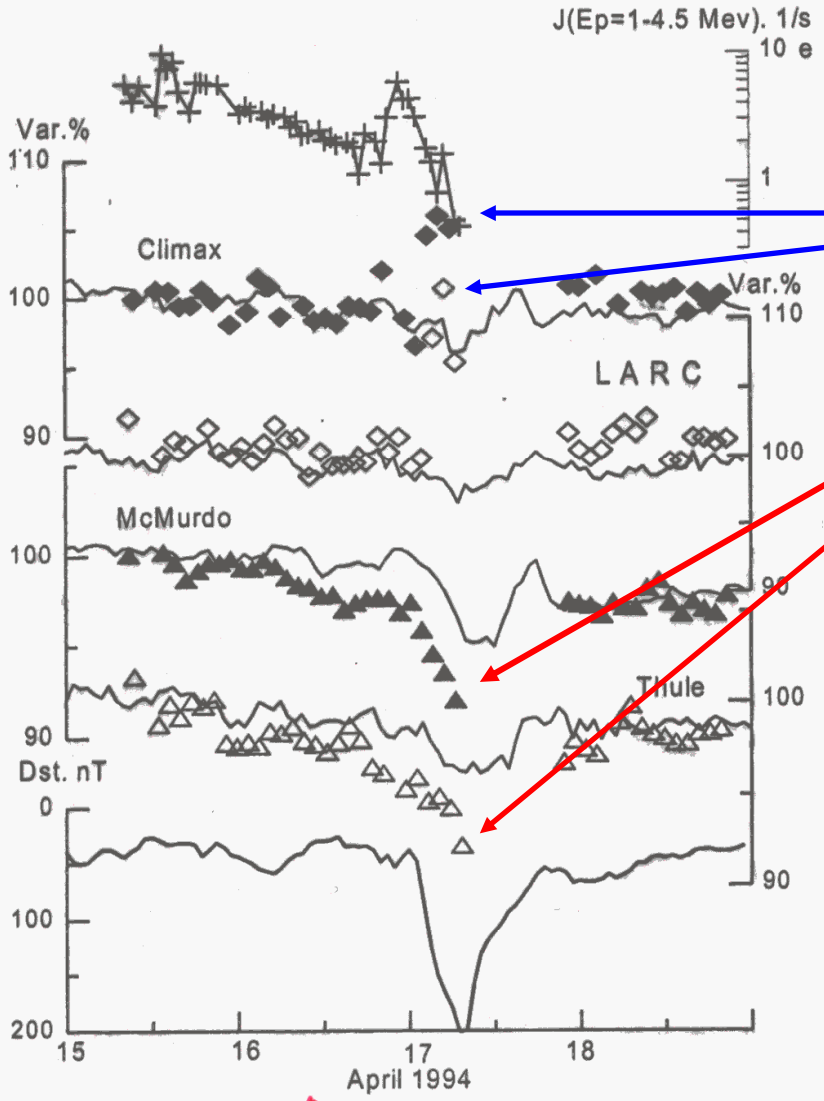

Fig. SONG instrument's (CORONAS-I satellite, protons E >50 MeV with geometrical factor 2000 cm^2 x sr) counting rate, obtained in the polar caps (triangles) and at the middle latitudes (diamonds) and NM data for April 15-18, 1994. For each orbit the selection of L corresponds to the position of the NMs (Kuznetsov et al., 2002)

500 km, polar orbit

Increase of geomagnetic transmissivity at low orbits leads to observations of increase of GCR on satellite at middle latitudes during a Forbush decrease (FD observed well especially at high latitudes) *if instrument with large geometrical factor is used for high energy protons on satellite* (from *Kuznetsov, S.N. et al., J. Atmos. Sol. Terr. Physics, 64, Iss. 5-6, 535-539, 2002)*, CORONAS-I satellite.

2.2. Solar neutrons and gamma rays observed on satellites.

Hard X rays, gamma rays and neutrons, produced in acceleration processes in solar flares, and ***not affected by IMF or geomagnetic field***, are measured on satellites.

Informations provided by the high energy photons as the products of interactions of charged particles accelerated in the solar flares, are summarized e.g. in paper *(G.H. Share, R.J. Murphy, Geophys. Monograph Ser. 162, 1029/162GM20, 2005 and references therein).*

e^- *produce bremsstrahlung with continuous spectrum*

accelerated nuclei produce n, gamma ray lines caused by deexcitation of nuclei, e^+*,radioactive nuclei etc*

ions accelerated to *very high energy* (~100 MeV) produce pions with subsequent decay and emission of e^-, e^+, and gamma rays (continuum radiation).

First indication of solar neutrons on satellite was reported from flare 21 June 1980 in SMM measurements (***Chupp, E.L. et al, ApJL, 263, L95, 1982*****).**

At present there exist ***detailed measurements of gamma rays up to 10 MeV including the deexcitation lines in the mission RHESSI*** *(e.g. D.M. Smith et al, ApJL, 595, L81-L84, 2003),* and in the project ***INTEGRAL*** *(J. Kiener et al, A&A, 445, 725-733, 2006).*

In the *energy range up to 100 MeV* there are available measurements from instrument ***SONG at the CORONAS-F*** satellite (*Kuznetsov, S.N. et al, Indian J. Radio Space Phys., 33, 353 - 357, 2004*). Data from this experiment are available from August 2001 until December 2005.

Review on solar flare gamma ray production is e.g. in paper (*Ramaty et al, Space Sci. Rev, 18, 341-388, 1975*) and in book (*Chupp, E.L., Gamma Ray Astronomy. Nuclear Transition Region, Kluwer, 1976*).

Part of *neutrons* produced in solar flares *is captured by nuclei*. If *captured by p*, the line *2.223 MeV* appears (from $^{1}H(n,\gamma)^{2}H$ *reaction*).

Neutrons escaping from Sun are also studied by protons produced in their decay (first report by *Evenson, P., P. Meyer and K.R. Pyle, Astrophys. J., 274, 875, 1983*). From measured spectrum of p, direct indication of escaping neutrons can be obtained.

Positrons (e^{+}) in solar flares result from decay of radioactive β^{-} emitting nuclei (e.g. ^{11}C, ^{13}N etc.), de-excitation of nuclei (e.g. ^{16}O) and decay of π^{+} mesons, all of which are produced due to interactions of accelerated p (or heavier nuclei) with ambient solar atmosphere. Direct annihilation produces two γ quanta per e^{+} (0.511 MeV).

Various nuclear *de-excitation lines* are produced *by accelerated p* and heavier nuclei. The *strongest narrow lines:* 6.129 MeV (^{16}O), 4.438 MeV (^{12}C), 2.313 MeV (^{14}N), 1.779 MeV (^{28}Si), 1.634 MeV (^{20}Ne).

Proton spectra can be deduced from gamma ray and neutron observations. More can be found e.g. in paper (*Ramaty,R., R.J. Murphy, Space Science Rev., 45, 213-268, 1987*).

There were observed ***several high energy gamma ray and solar neutron events from flares by SONG on CORONAS-F satellite*** (*Kuznetsov S.N. et al., Proc. ICRC Tsukuba, 2003*) including those of October 28, and Nov. 4, 2003. High energy gamma rays were observed also in January 20, 2005 flare (*Kuznetsov S.N. et al., Proc. 29th ICRC (Pune), 1, 49-52, 2005*).

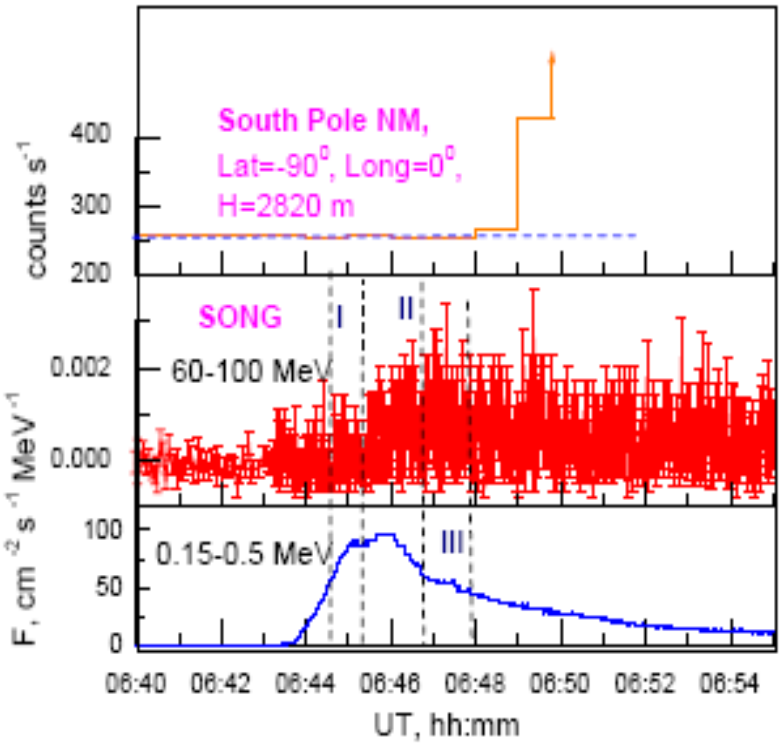

Figure 2. The temporal profile of measurements at two gamma ray channels of SONG along with the onset of GLE observed on South Pole NM.

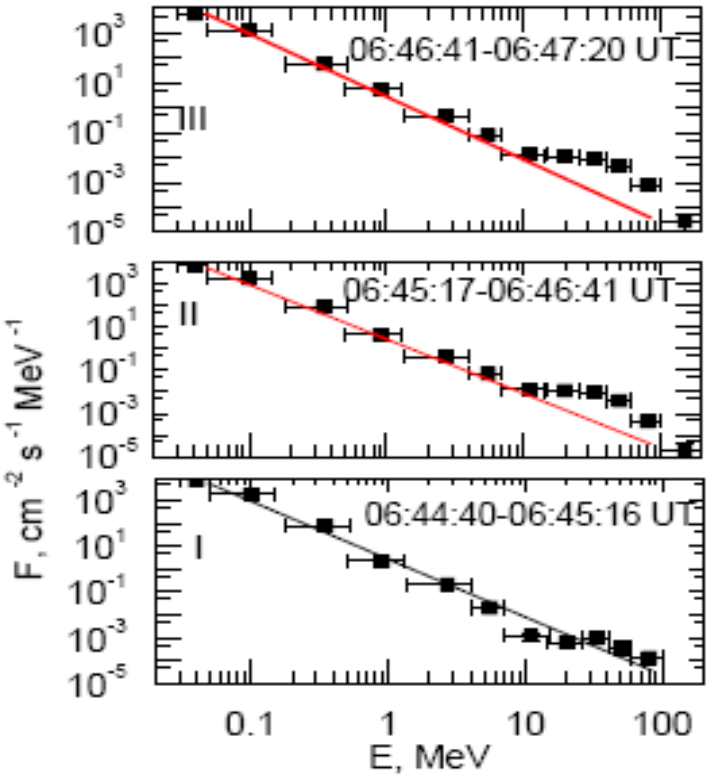

Figure 3. The energy spectra of gamma rays observed by SONG during three time intervals marked in Figure 2.

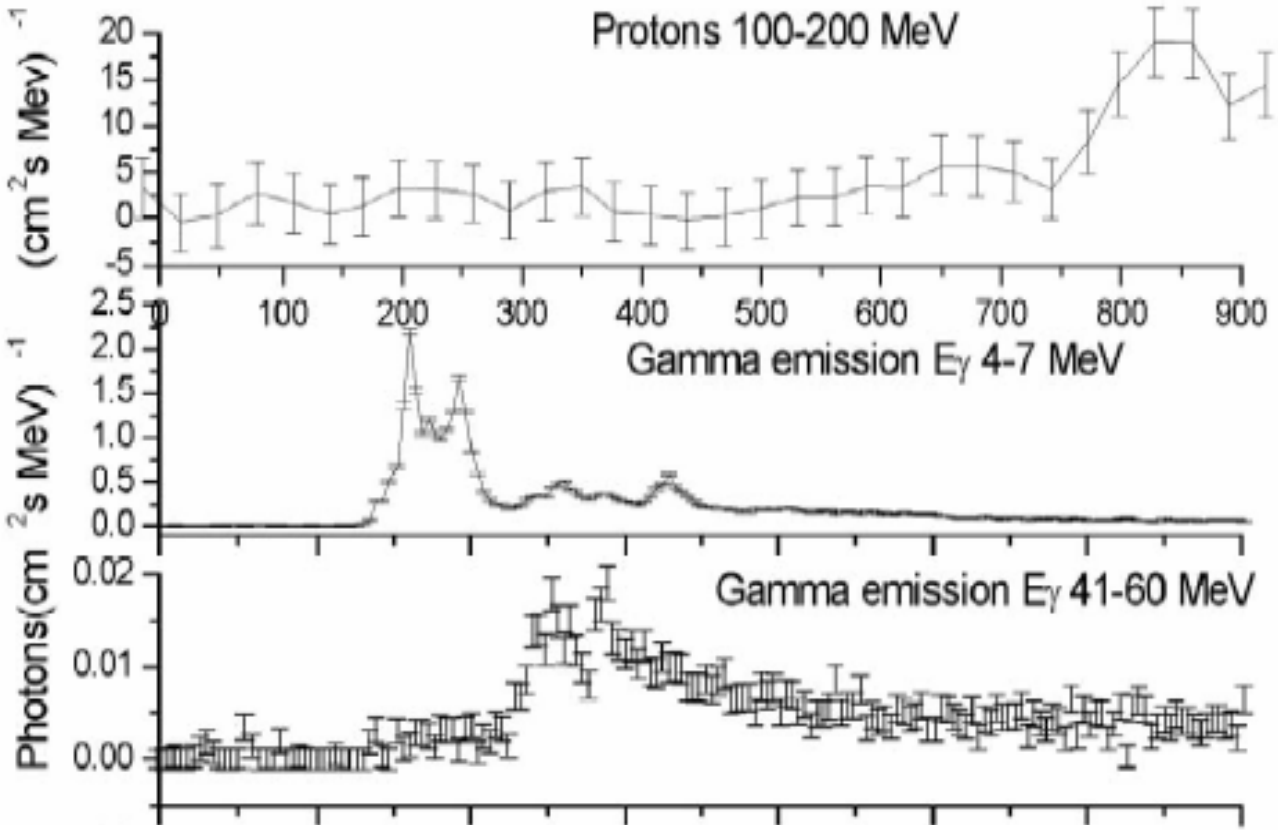

SONG/CORONAS-F during ***the solar flare October 28, 2003***. Change of energy spectra in time (sec after 11:00 UT) is apparent. Protons measured on the same satellite arrived later. L.Stit NM recorded p onset at 1115 UT.

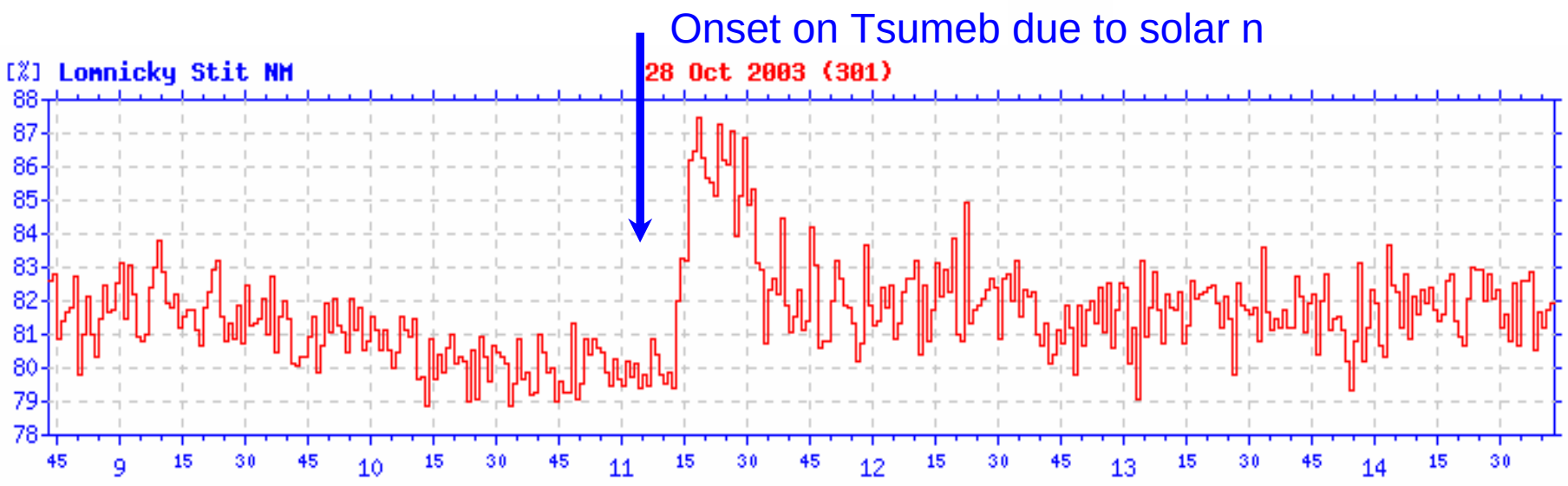

2.3. Transmissivity computed for low earth orbits.

There are *differences* of transmissivity function *at low earth orbit* for different *geomagnetic field models* and for different *levels of geomagnetic activity.*

Using tables of asymptotic directions and vertical cut-off rigidities computed in IGRF field (*Shea, M.A., D.F. Smart, Environ. Res. Pap. 503, AFCRL-TR-75-0185, pp165, Bedford, Mass., 1975*), the vertical cut-offs for altitudes > 20 km were approximated by (*Heinrich,W. and Spill,A., J. Geophys. Res., 84, A8, 4401-4404, 1979*) by using the approximation

$$R_c(1)/R_c(2)=L^2(1)/L^2(2)$$

where $R_c(1)$ and $R_c(2)$ are vertical cut-off values on the same radius vector from the center of earth and L is McIlwain parameter of the magnetic field shell.

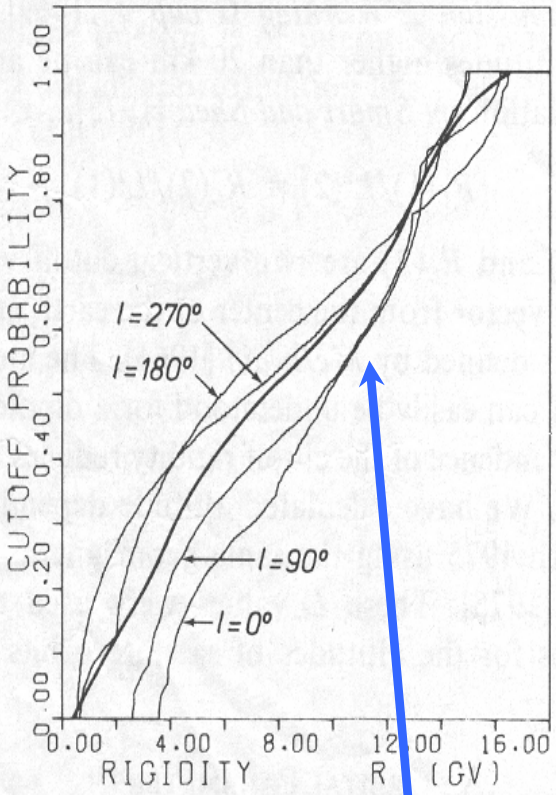

Fig. 1. Cutoff probability for a circular orbit (Apollo-Soyuz Test Project). Here $a = 223$ km, $\epsilon = 0$, and $i = 51.8°$. The weak curves are cutoff probabilities averaged over the time of one revolution for sub-satellite tracks intersecting the equator at $I = 0°$, 90°, 180°, and 270°. The solid curve shows the cutoff probability averaged over the whole mission.

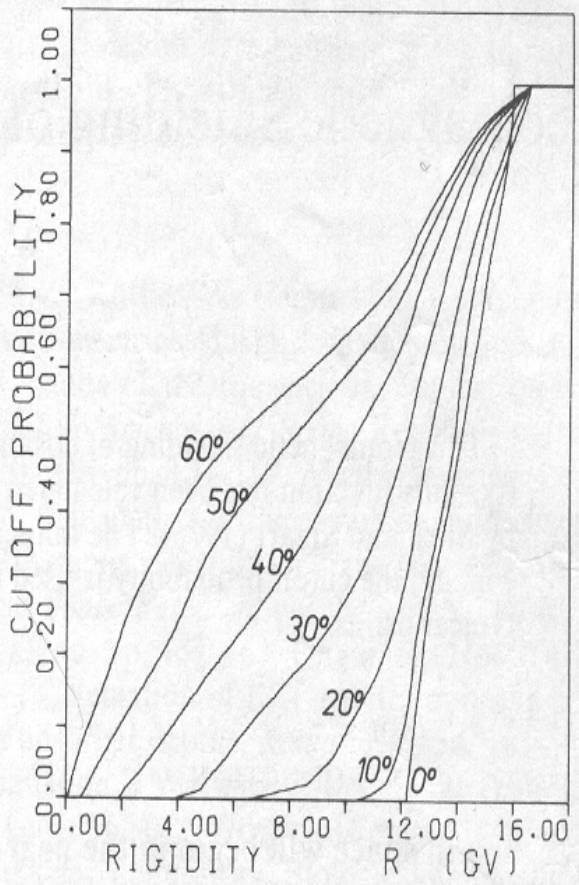

Fig. 2. Averaged cutoff probability for a circular orbit ($a = 223$ km). Parameter of the curves is the inclination angle.

Vertical cut-off probabilities at low earth orbit (from paper by *Heinrich,W. and A. Spill, JGR, vol. 84, A8, 4401-4404, 1979*).

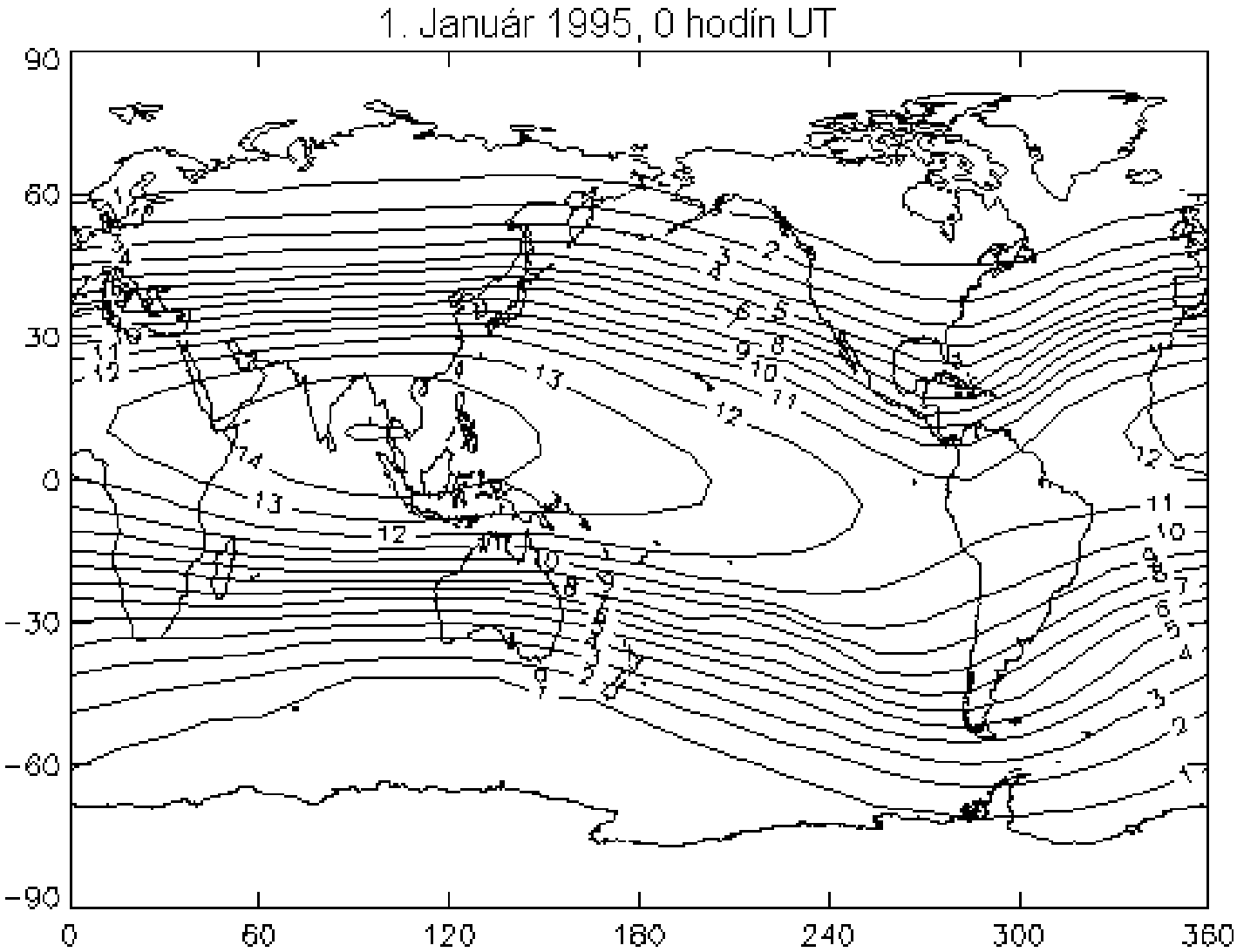

Map of vertical cut-off rigidities computed for AMS with Ts'89 external field, lowest geomagnetic activity level, from grid 5 x 15 degrees (lat x long), (*Bobík, P., PhD thesis, 2001*)

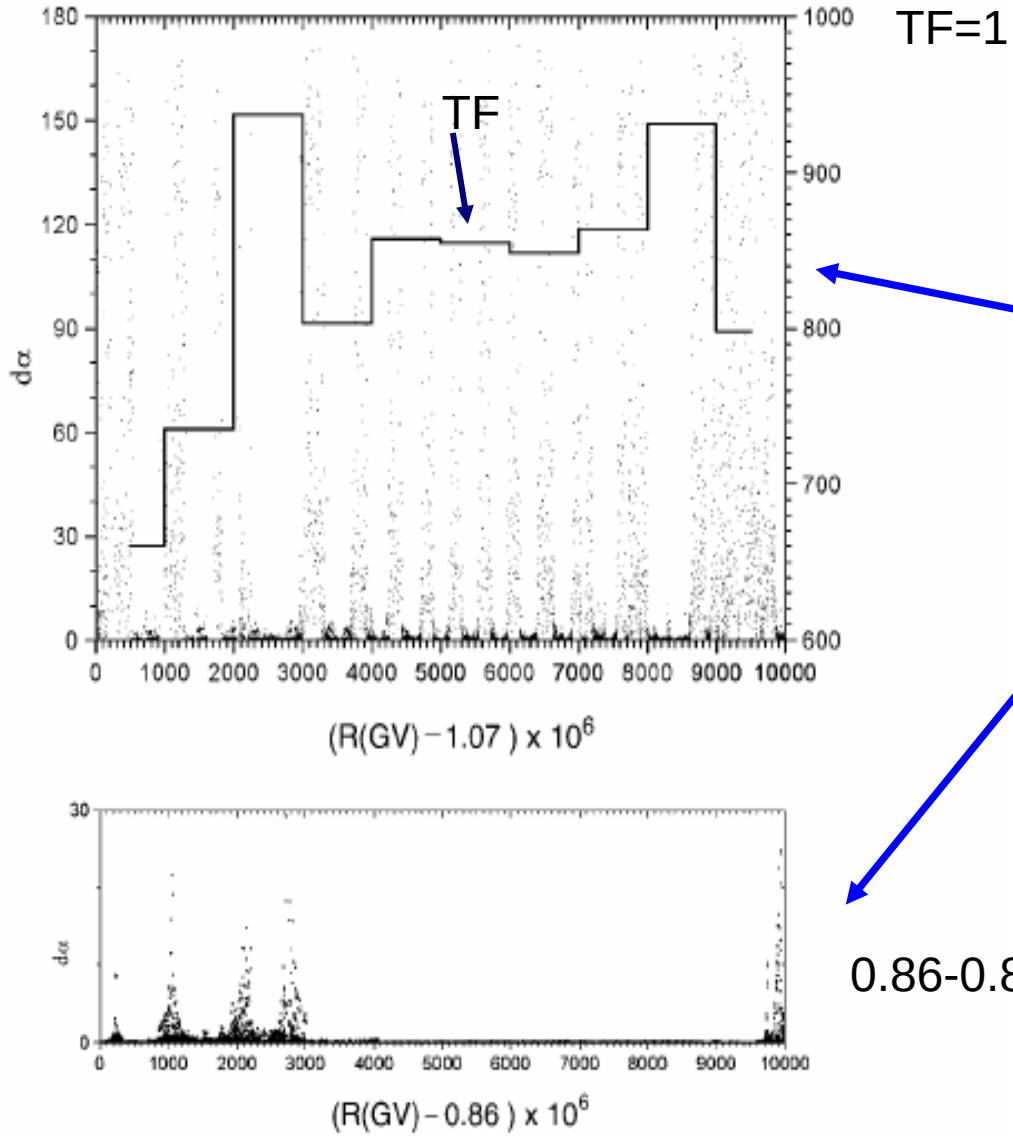

During the strong disturbances the penumbra at low altitudes has rather complicated structure (*Kudela, K. and I.G. Usoskin, Czech. J. Phys,54, 239-254, 2004*). There appear windows for relatively low rigidities.

Fig. 7. Fine structure of the penumbra at the altitude of 500 km above the position of LARC neutron monitor calculated using the Ts89 model with *Dst* extension −300 nT. Rigidity intervals of (1.07–1.08) GV (upper panel) and (0.86–0.87) GV (lower panel) are depicted. The angular difference dα of two subsequent asymptotic directions is displayed by dots (labeled left axis, in degrees, similar value as in Fig. 1). Solid line and the right axis in the upper panel correspond to the computed transmissivity function. $TF = 1$ for the lower panel.

TFs computed for AMS experiment during the flight in June 1998 (*Bobík, P. et al., 2006, JGR*) for different regions indicated in Table 1.

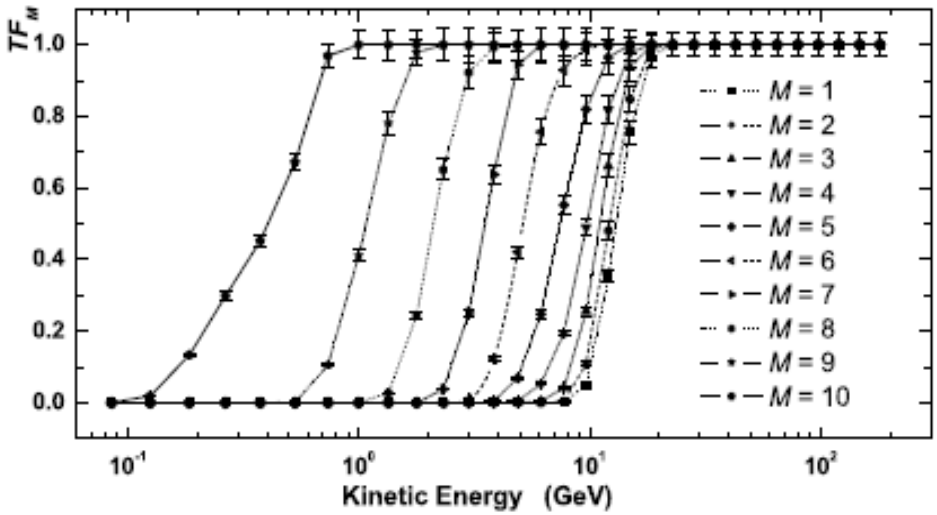

Figure 1. Transmission Function, TF_M, evaluated for AMS-01 regions during the STS-91 mission flight time (June 1998) as a function of the proton kinetic energy in GeV. The lines are to guide the eye.

Table 1. Geomagnetic regions covered by AMS-01 measurements and kinetic energies corresponding to the dip for each geomagnetic zone (see [*AMS Collaboration*, 2000a; *AMS Collaboration*, 2002]). The regions are defined using the Corrected Geomagnetic latitude (CGM).

Region (M)	CGM latitude θ_M (rad)	Kinetic energy (GeV)
1	$\lvert\theta_M\rvert \leq 0.2$	6.16
2	$0.2 \leq \lvert\theta_M\rvert \leq 0.3$	6.16
3	$0.3 \leq \lvert\theta_M\rvert \leq 0.4$	4.88
4	$0.4 \leq \lvert\theta_M\rvert \leq 0.5$	3.00
5	$0.5 \leq \lvert\theta_M\rvert \leq 0.6$	3.00
6	$0.6 \leq \lvert\theta_M\rvert \leq 0.7$	1.78
7	$0.7 \leq \lvert\theta_M\rvert \leq 0.8$	1.35
8	$0.8 \leq \lvert\theta_M\rvert \leq 0.9$	0.74
9	$0.9 \leq \lvert\theta_M\rvert \leq 1.0$	0.27
10	$\lvert\theta_M\rvert \geq 1.0$	0.07

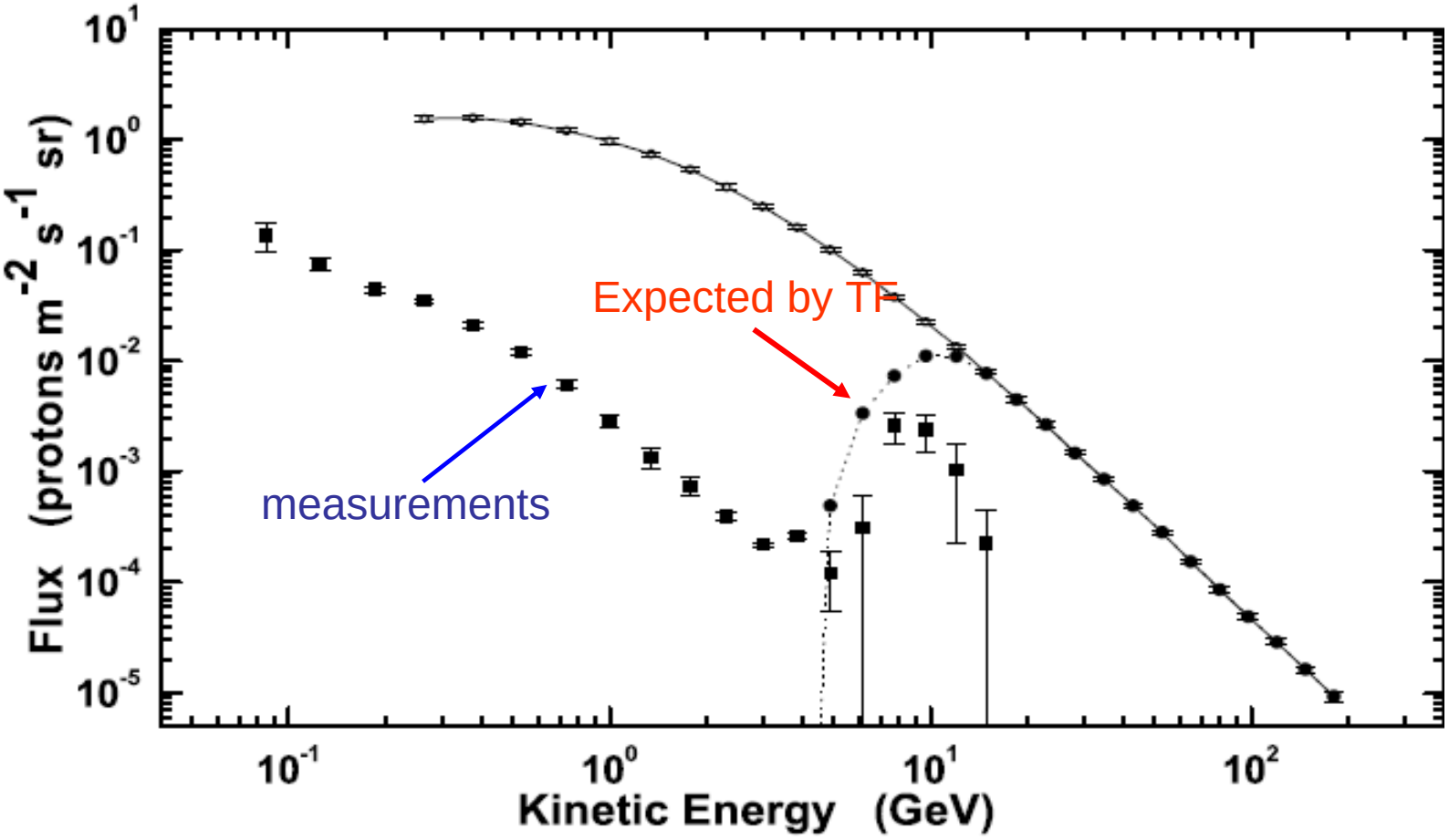

Figure 5. Fluxes per units of solid angle as a function of the proton kinetic energy for the 4th geomagne
(○) $\Phi^{1AU}(R_b)$, (●) $\Phi_4(R_b)$ and (■) $\Phi_4^s(R_b)$. The lines are to guide the eye.

In penumbra region the observed energy spectra showed the excess above those predicted by primary cosmic ray (CREME96 model) and TF function computed. This allows to estimate contribution of secondary cosmic rays (mainly re-entrant albedo protons).

Recent paper *Advances in Space Research*, *Volume 37, Issue 6*, *2006*, *Pages 1206-1217*

A geomagnetic cutoff rigidity interpolation tool: Accuracy verification and application to space weather

D.F. Smart [a,*], M.A. Shea [a], A.J. Tylka [b], P.R. Boberg [b,c]

provides useful tool for vertical cut-offs estimates having *general space weather applications*. It is compared with SAMPEX measurements for several solar particle events under a variety of geomagnetic conditions. *Predicted cut-off latitudes are with one degree of the observed latitudes for quiet times* (figures taken from that paper).

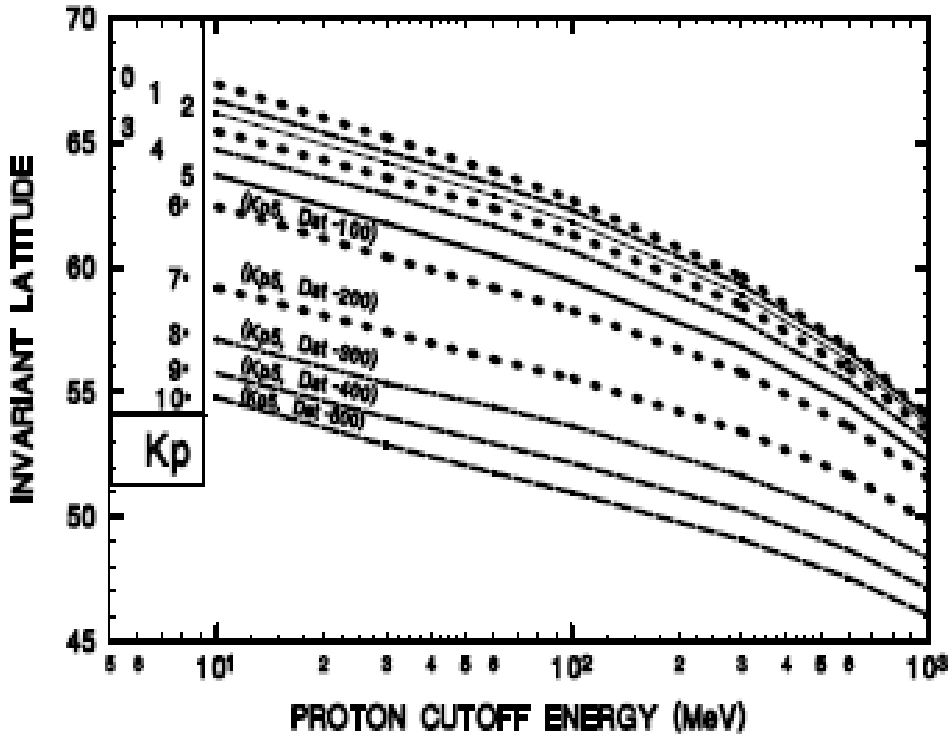

Fig. 1. The average (of all local times) change in proton cutoff energy as function of the Kp magnetic index.

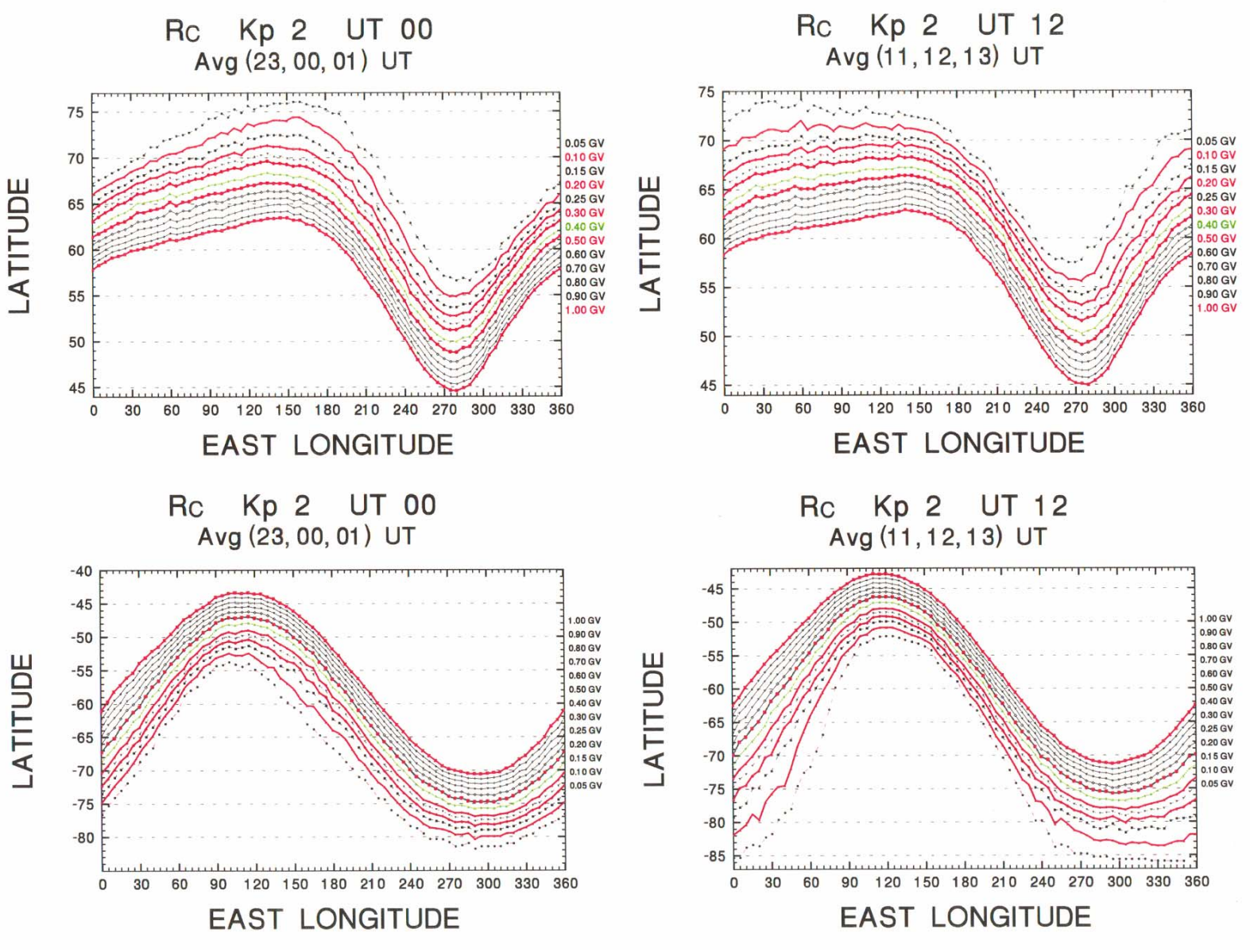

Lines of constant vertical cut-offs for low geomagnetic activity in geographic coordinates (upper and lower panels - north and south hemisphere) for noon and midnight (*Smart, D.F. et al., Adv. Space Res., 2006*) at 450 km orbit.

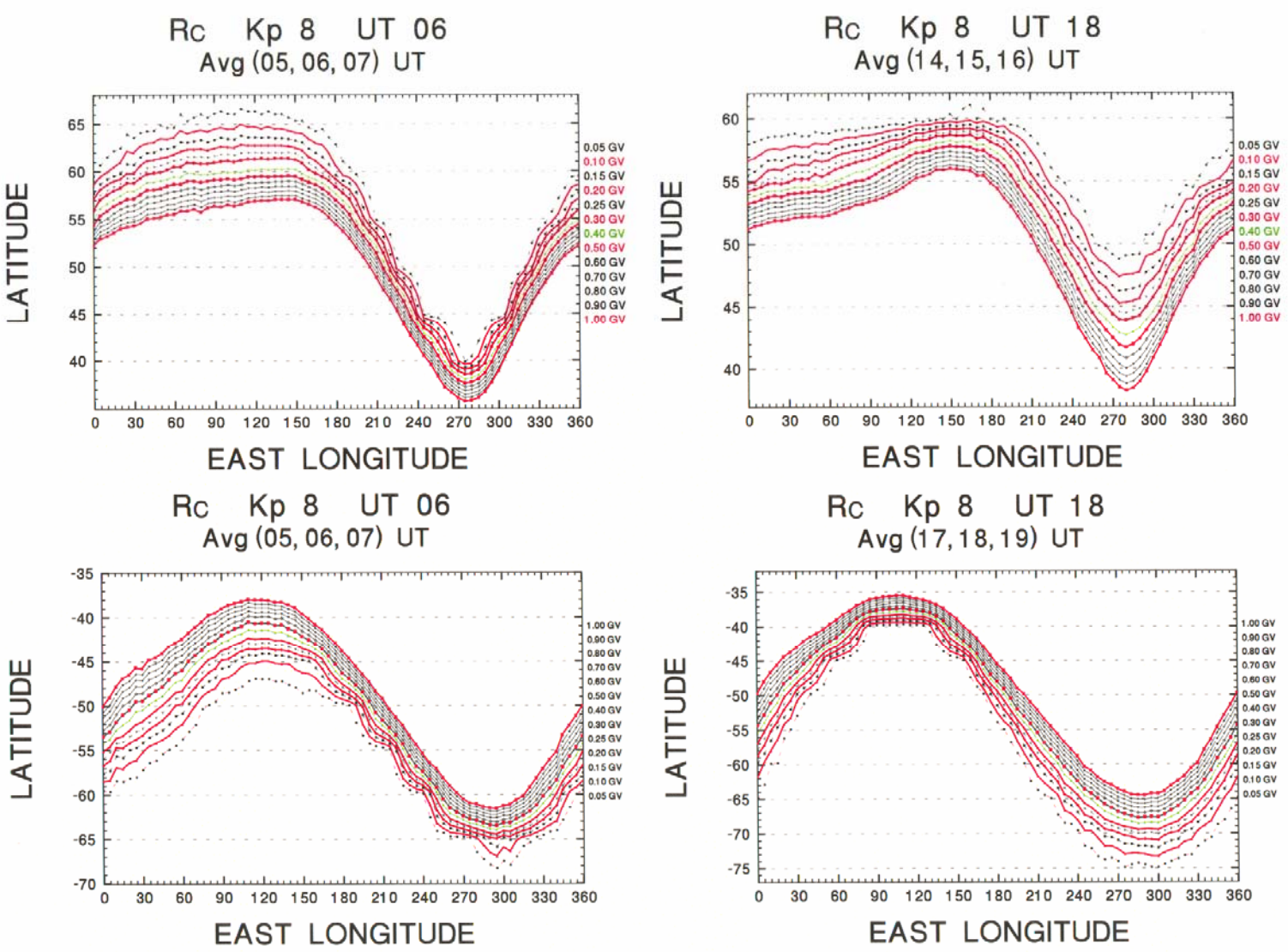

Lines of constant vertical cut-offs for high geomagnetic activity in geographic coordinates (upper and lower panels - north and south hemisphere) for dawn and dusk (*Smart, D.F. et al., Adv. Space Res., 2006*) at 450 km orbit.

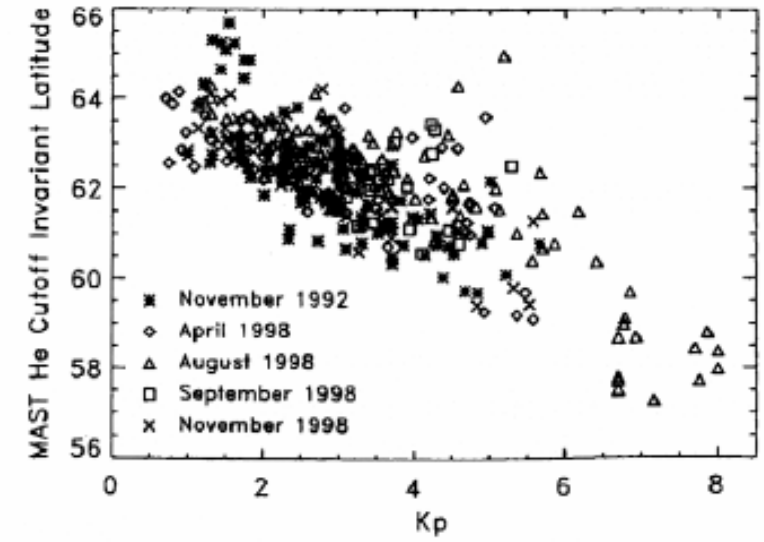

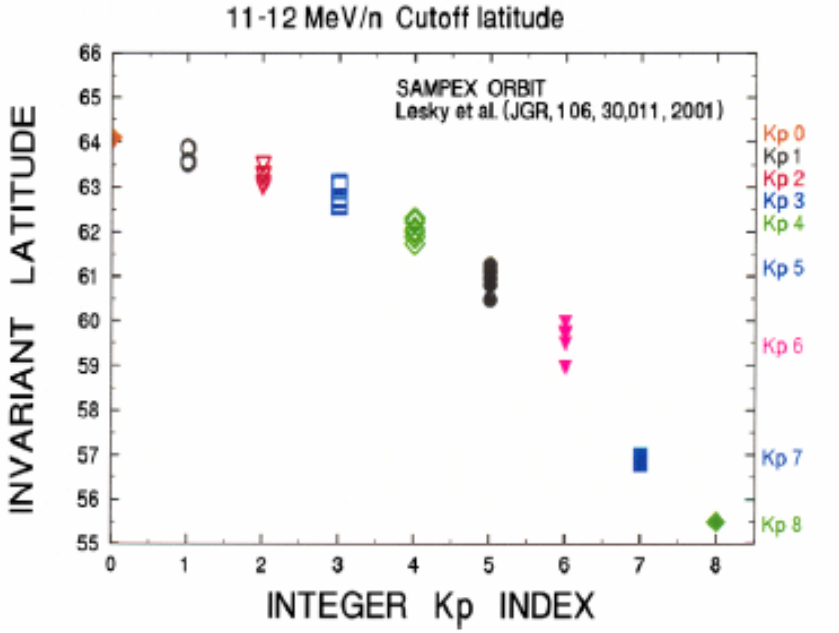

Fig. 9. Comparison of the measured and computed average invariant cutoff latitude. Top: the event summary cutoff latitude measured by SAMPEX. (Reproduced from Leske et al. (2001) by permission of the American Geophysical Union.) Bottom: the event-averaged computed cutoff latitude for 11.5 MeV/*n* α particles (0.294 GV) from this work.

Copied from paper by *Smart D.F. et al., Adv. Space Res. 2006*.
From trajectory calculations in IGRF+Ts field model a library of vertical geomagnetic cutoffs for all magnetic conditions is represented.
Accuracy of this interpolation by comparing with SAMPEX data is demonstrated.